Lecture 2
Parameter estimation of specular components in channel impulse responses

Xuefeng Yin

Multipath Propagation Environment

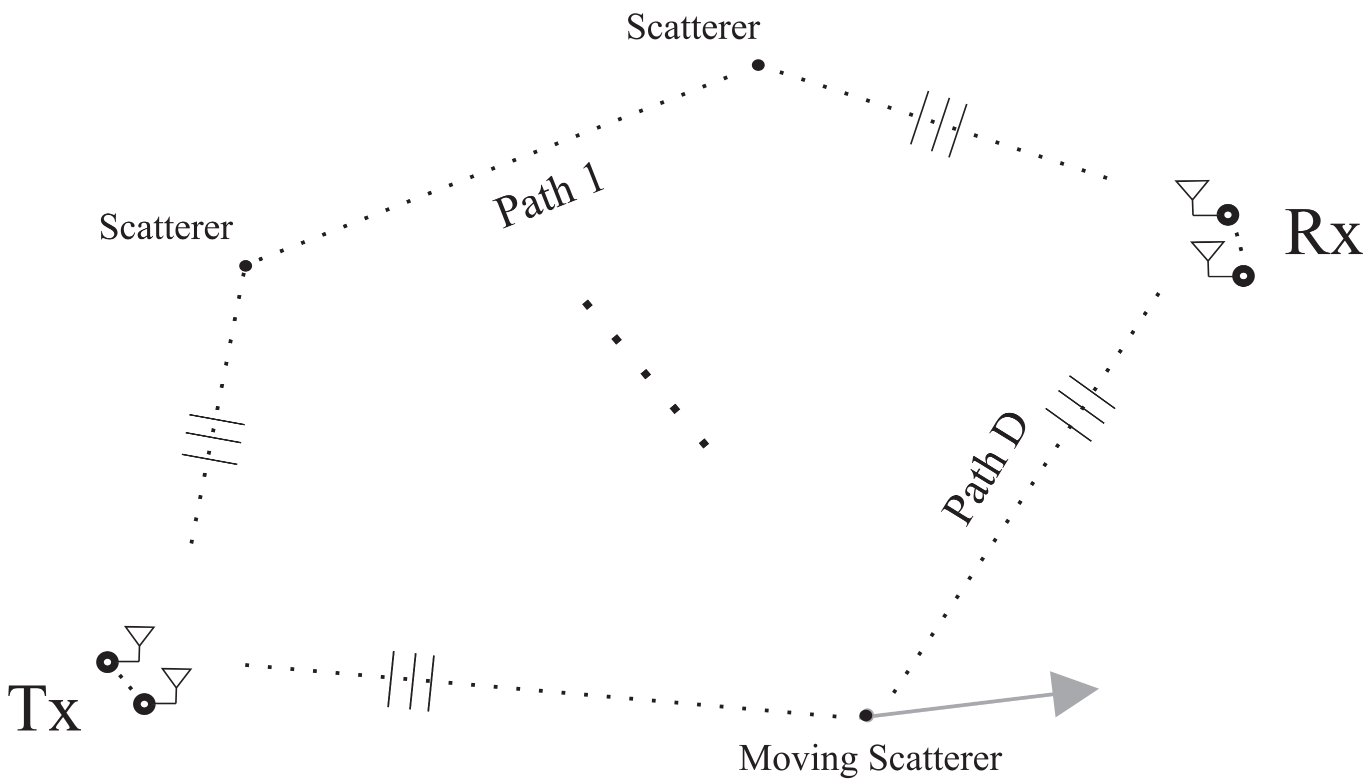

- Dispersion dimensions : delay, direction of departure (DoD), direction of arrival (DoA), polarizations and Doppler frequency
- Dispersion parameters of a propagation path:
  - center of gravity per dimension
- Time-evolution behavior of these parameters

An Experimental Example of the Dispersion of a Radio Channel

- MIMO channel sounder: Propsound
- Tx and Rx Arrays: 50-element omni-directional dual-polarized array
- 5.25 GHz Carrier frequency
- 100 MHz bandwidth

Tx trolley

Rx trolley

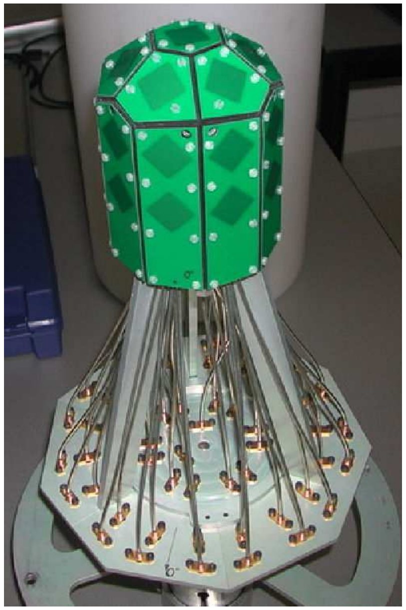

Tx/Rx Array

An experimental example: direction and delay dispersion of an indoor propagation channel

- Average delay power spectrum

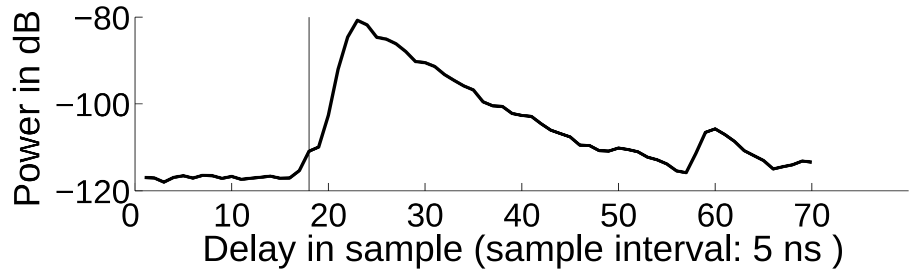

- Bartlett spectrum w.r.t. azimuth and elevation of departure at delay 90 ns:

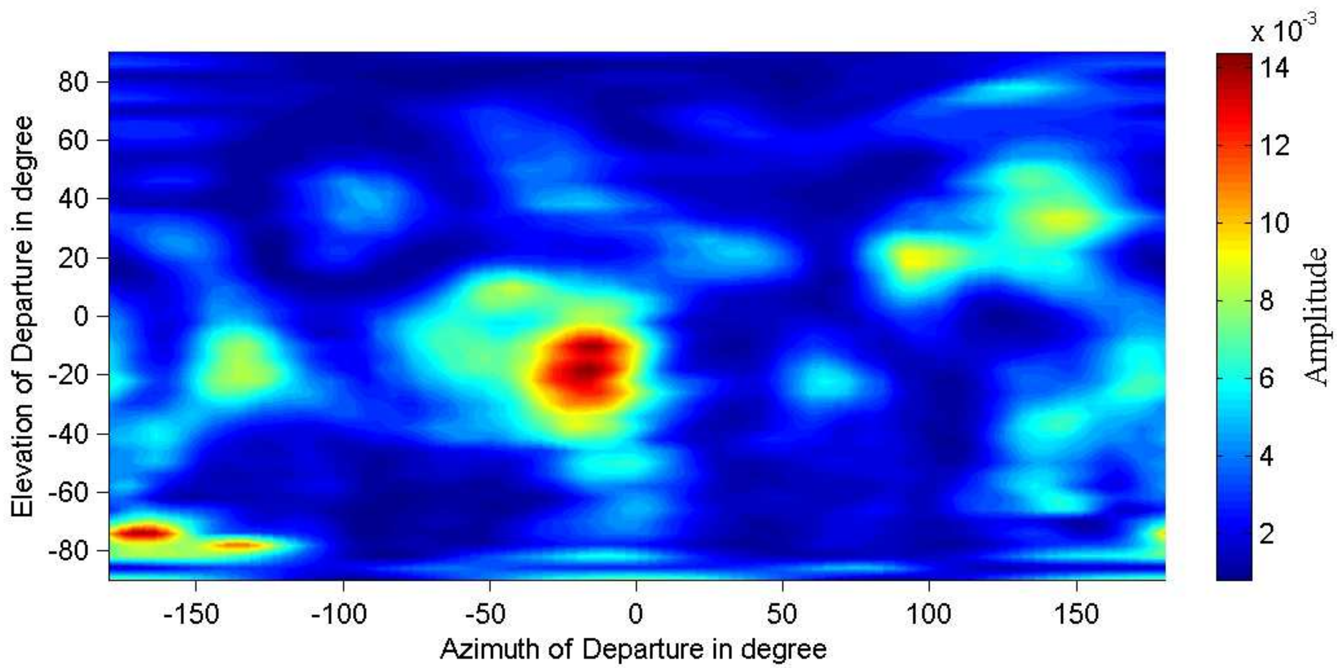

An experimental example: direction and delay dispersion of an indoor propagation channel

- Average delay power spectrum

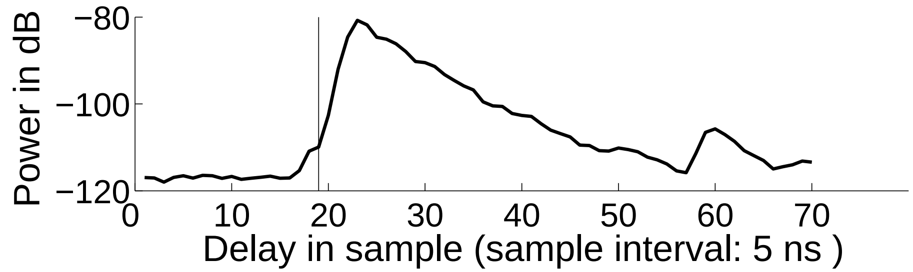

- Bartlett spectrum w.r.t. azimuth and elevation of departure at delay 95 ns:

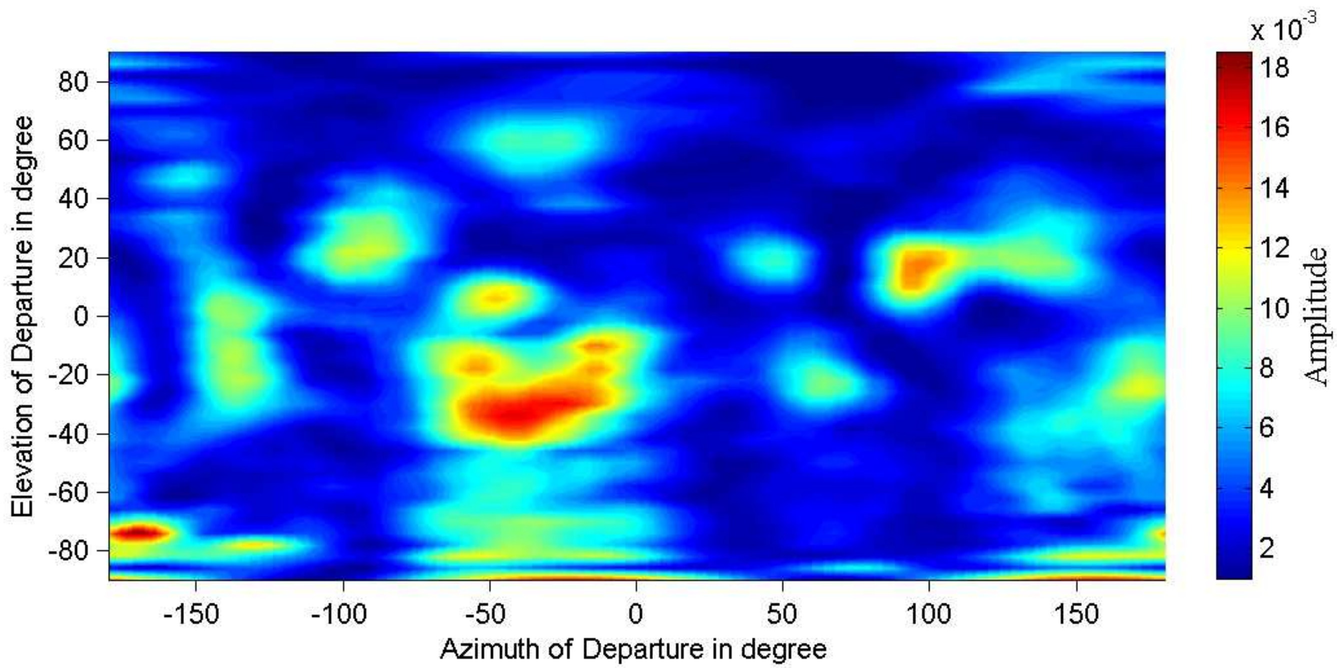

An experimental example: direction and delay dispersion of an indoor propagation channel

- Average delay power spectrum

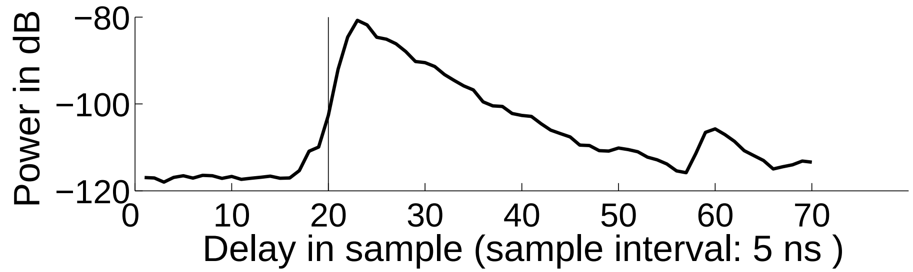

- Bartlett spectrum w.r.t. azimuth and elevation of departure at delay 100 ns:

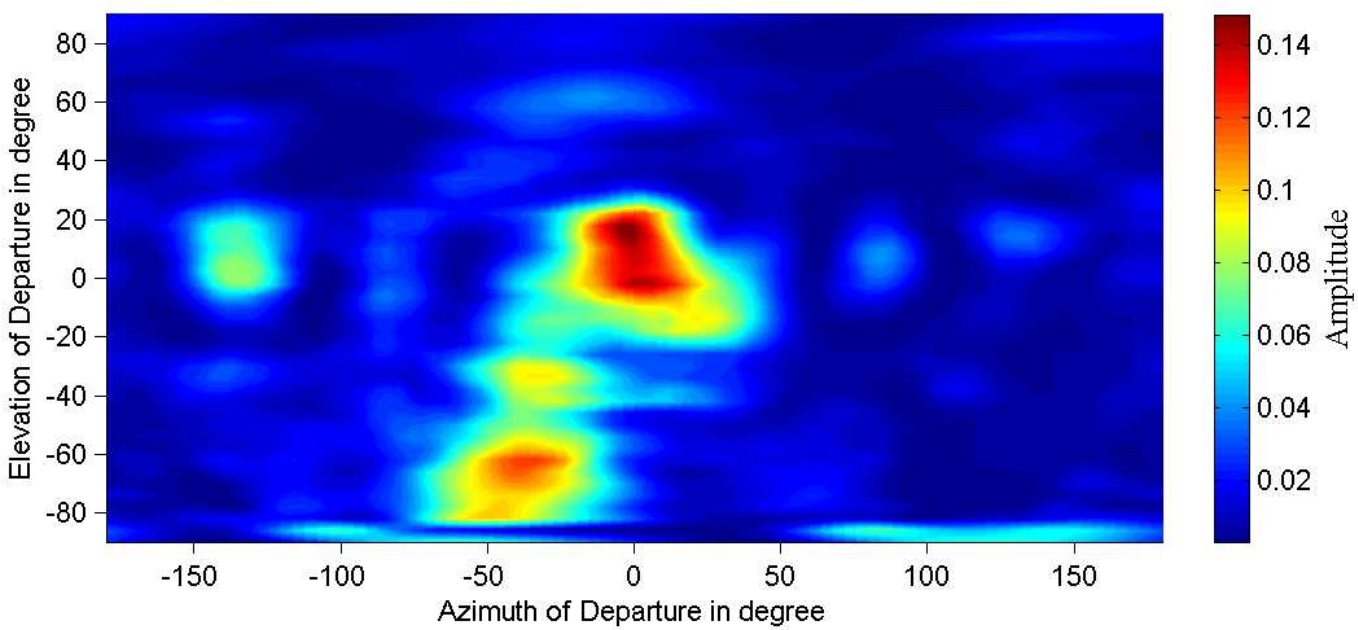

An experimental example: direction and delay dispersion of an indoor propagation channel

- Average delay power spectrum

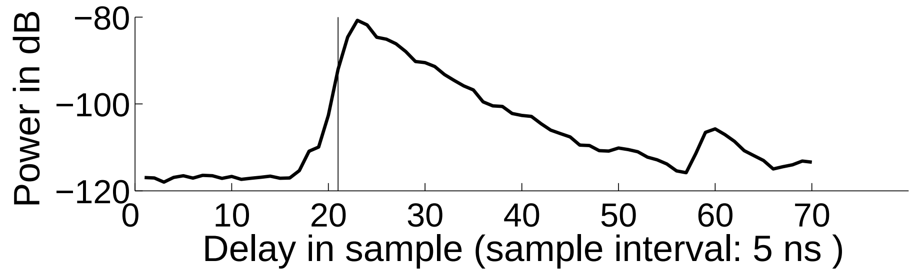

- Bartlett spectrum w.r.t. azimuth and elevation of departure at delay 105 ns:

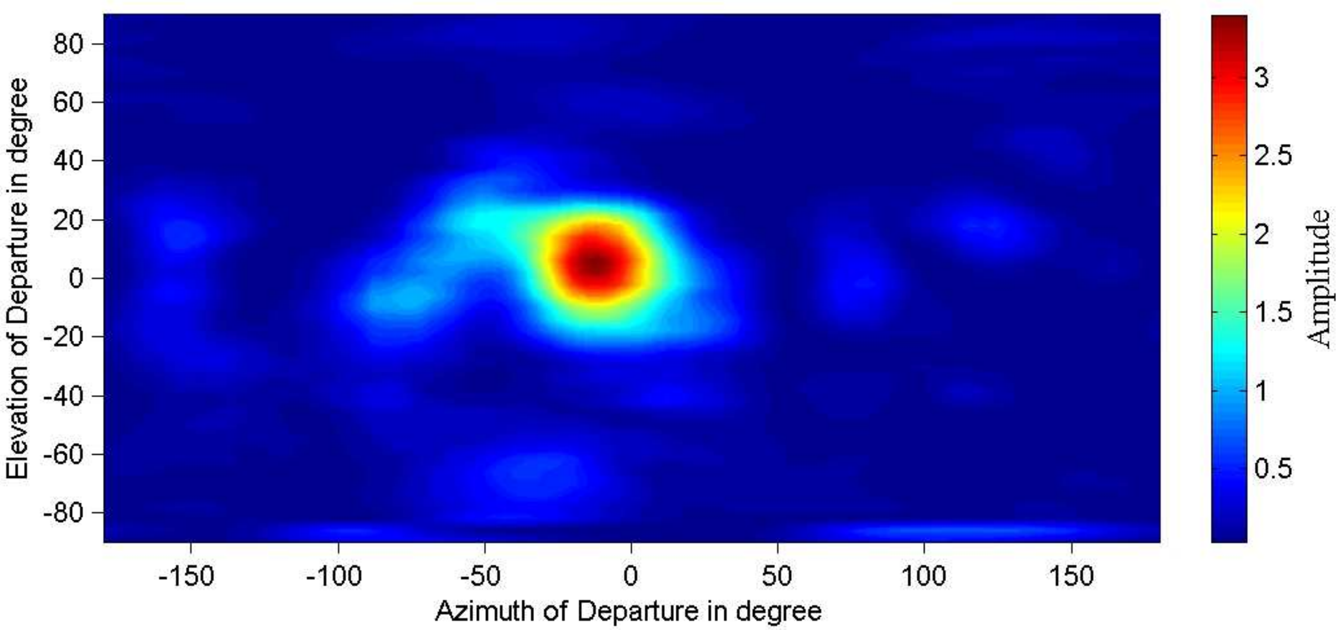

An experimental example: direction and delay dispersion of an indoor propagation channel

- Average delay power spectrum

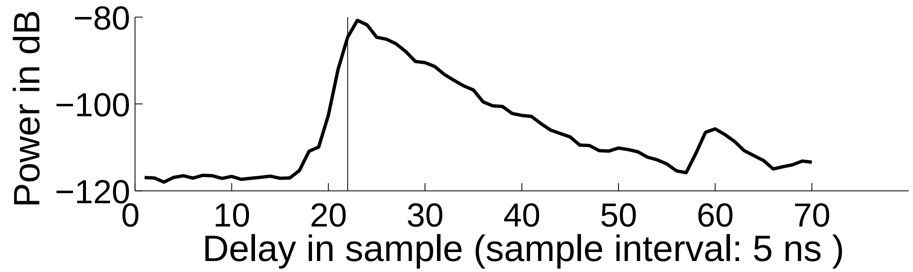

- Bartlett spectrum w.r.t. azimuth and elevation of departure at delay 110 ns:

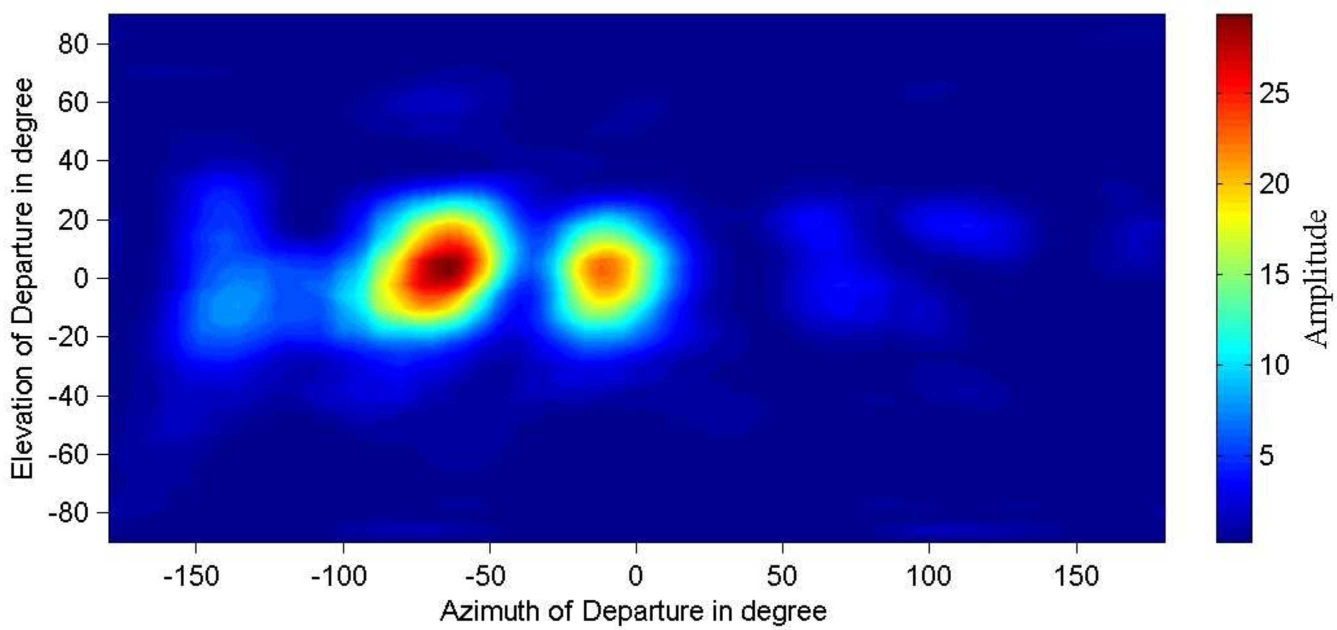

An experimental example: direction and delay dispersion of an indoor propagation channel

- Average delay power spectrum

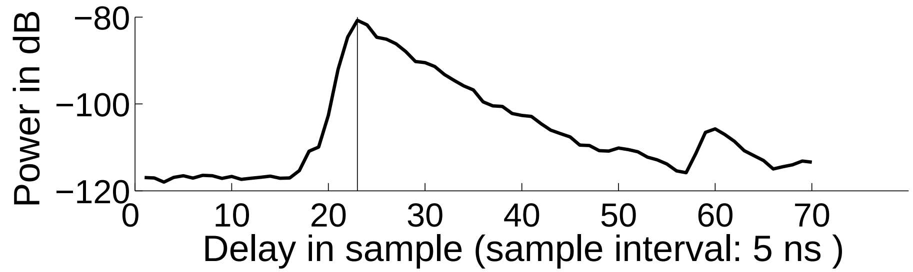

- Bartlett spectrum w.r.t. azimuth and elevation of departure at delay 115 ns:

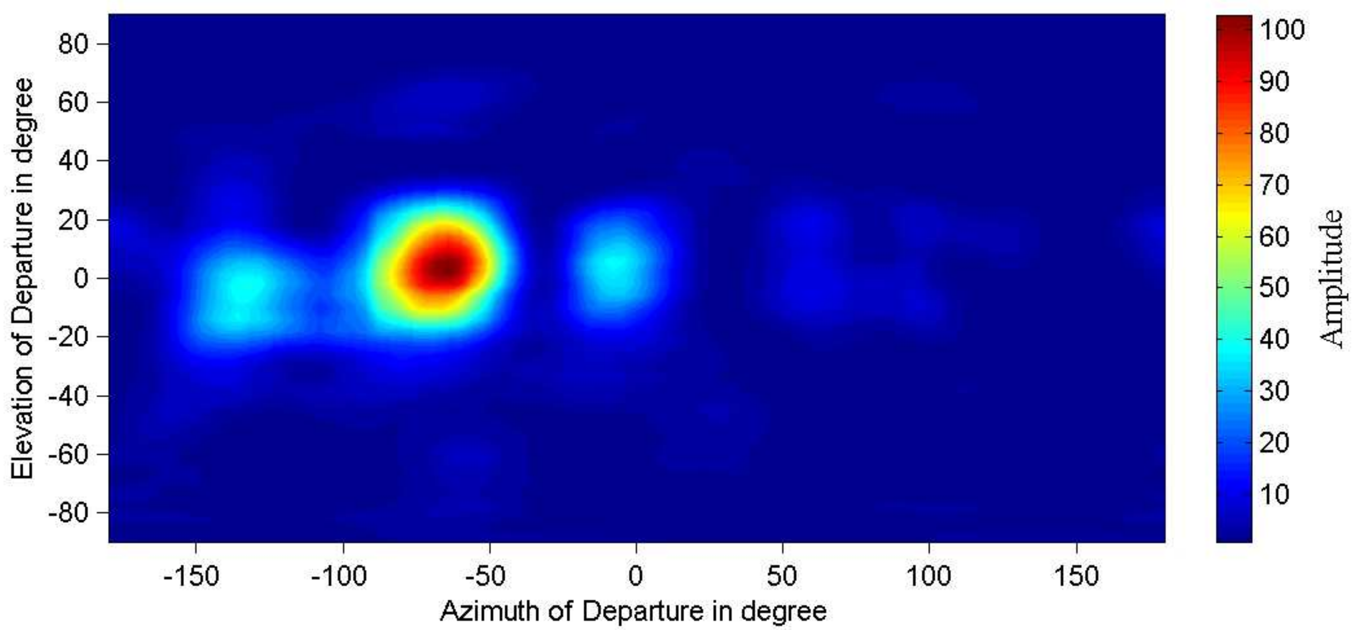

An experimental example: direction and delay dispersion of an indoor propagation channel

- Average delay power spectrum

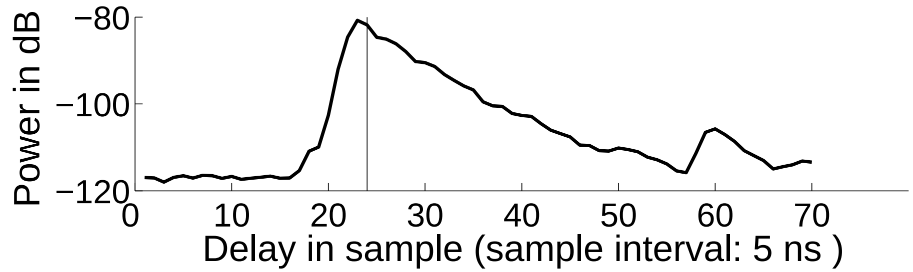

- Bartlett spectrum w.r.t. azimuth and elevation of departure at delay 120 ns:

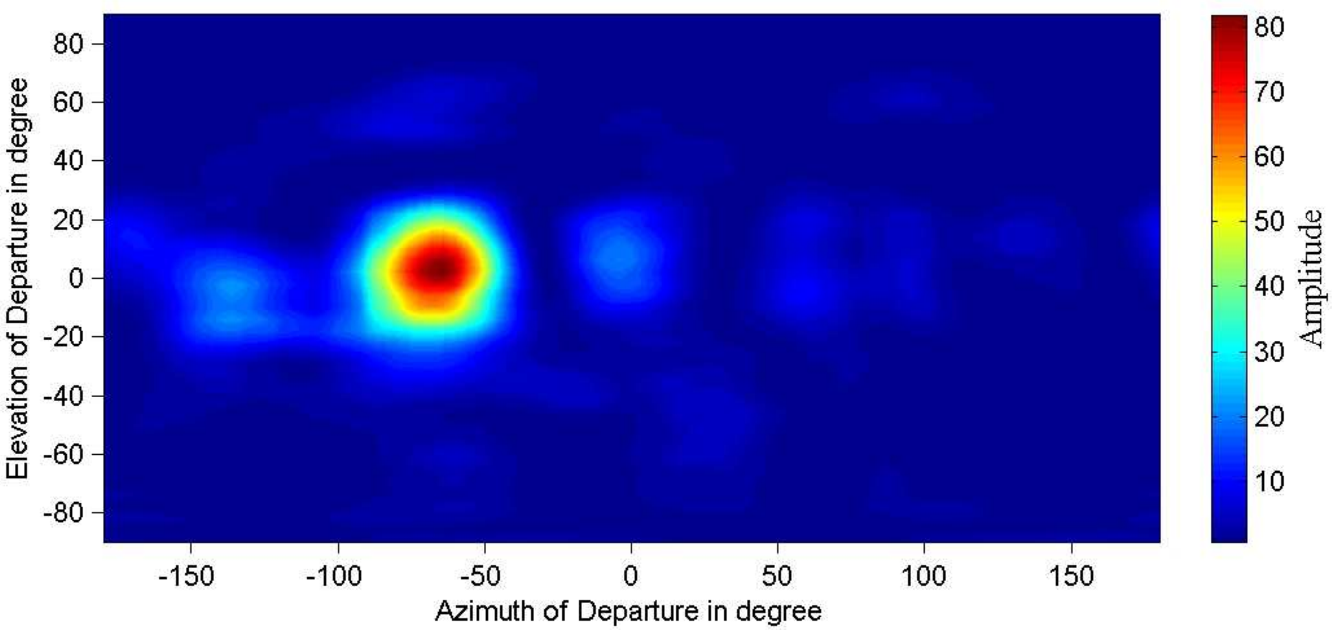

An experimental example: direction and delay dispersion of an indoor propagation channel

- Average delay power spectrum

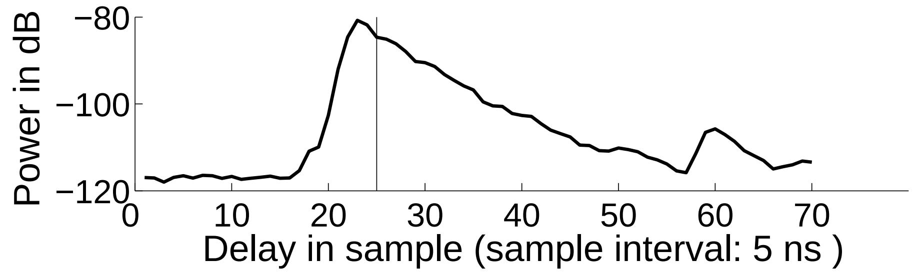

- Bartlett spectrum w.r.t. azimuth and elevation of departure at delay 125 ns:

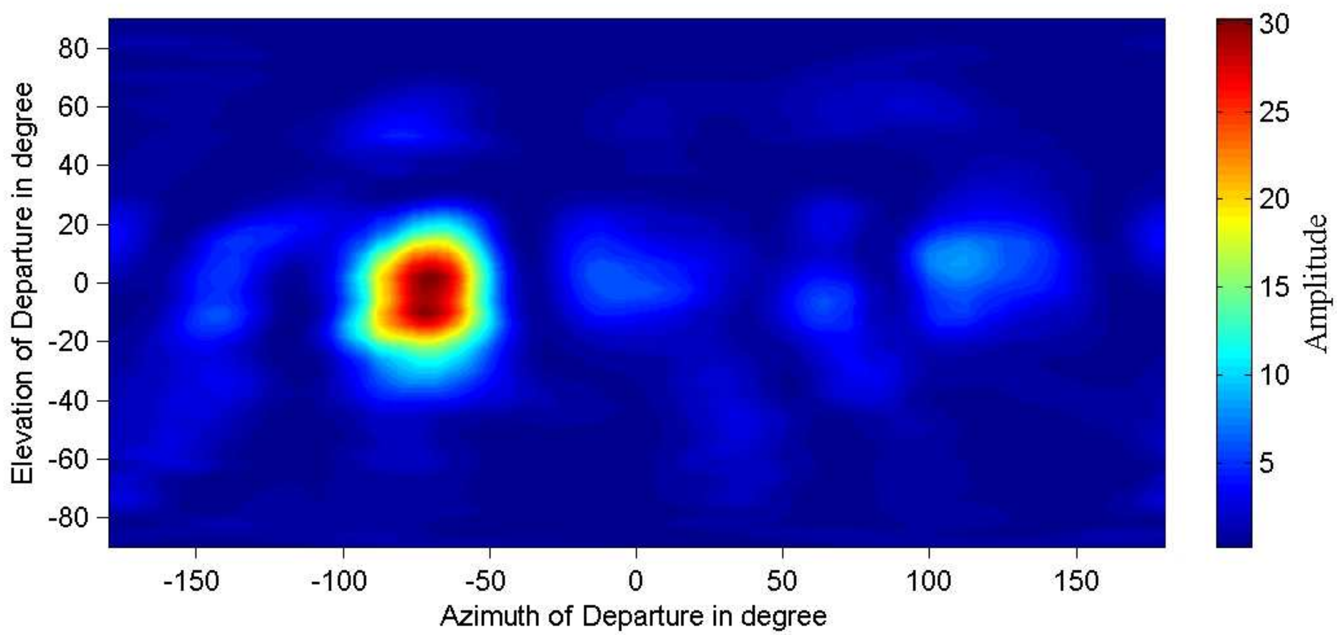

An experimental example: direction and delay dispersion of an indoor propagation channel

- Average delay power spectrum

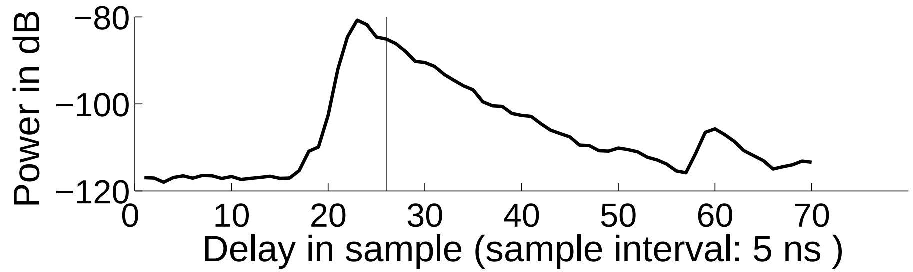

- Bartlett spectrum w.r.t. azimuth and elevation of departure at delay 120 ns:

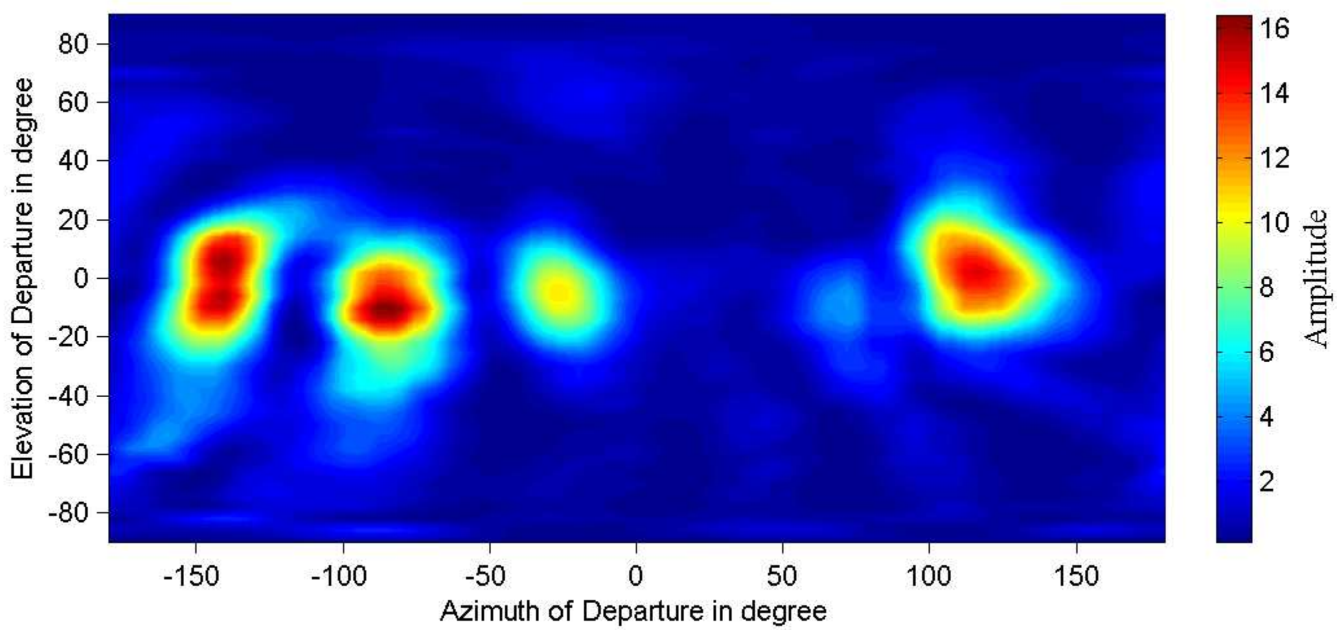

An experimental example: direction and delay dispersion of an indoor propagation channel

- Average delay power spectrum

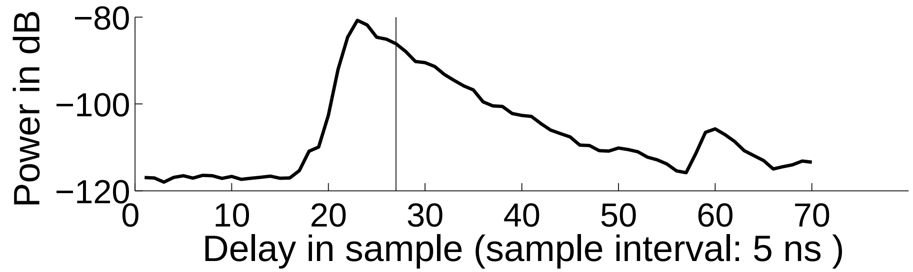

- Bartlett spectrum w.r.t. azimuth and elevation of departure at delay 135 ns:

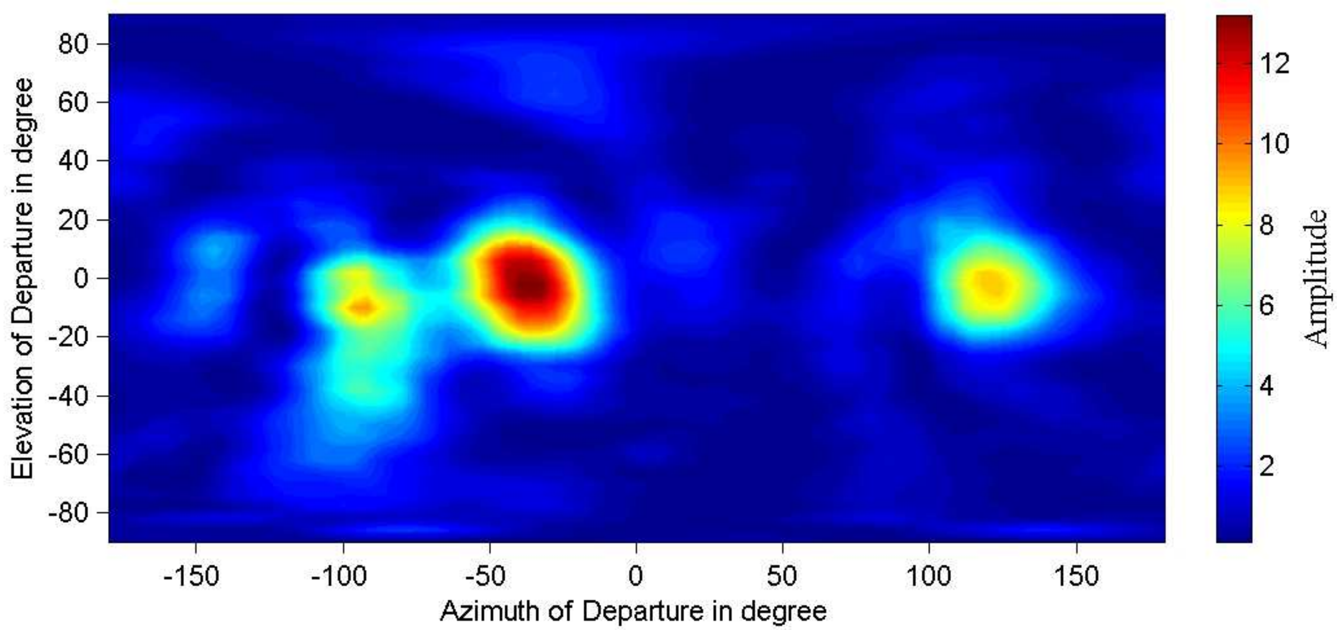

An experimental example: direction and delay dispersion of an indoor propagation channel

- Average delay power spectrum

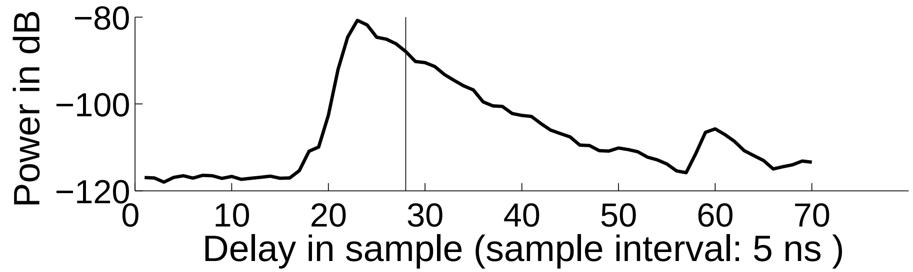

- Bartlett spectrum w.r.t. azimuth and elevation of departure at delay 140 ns:

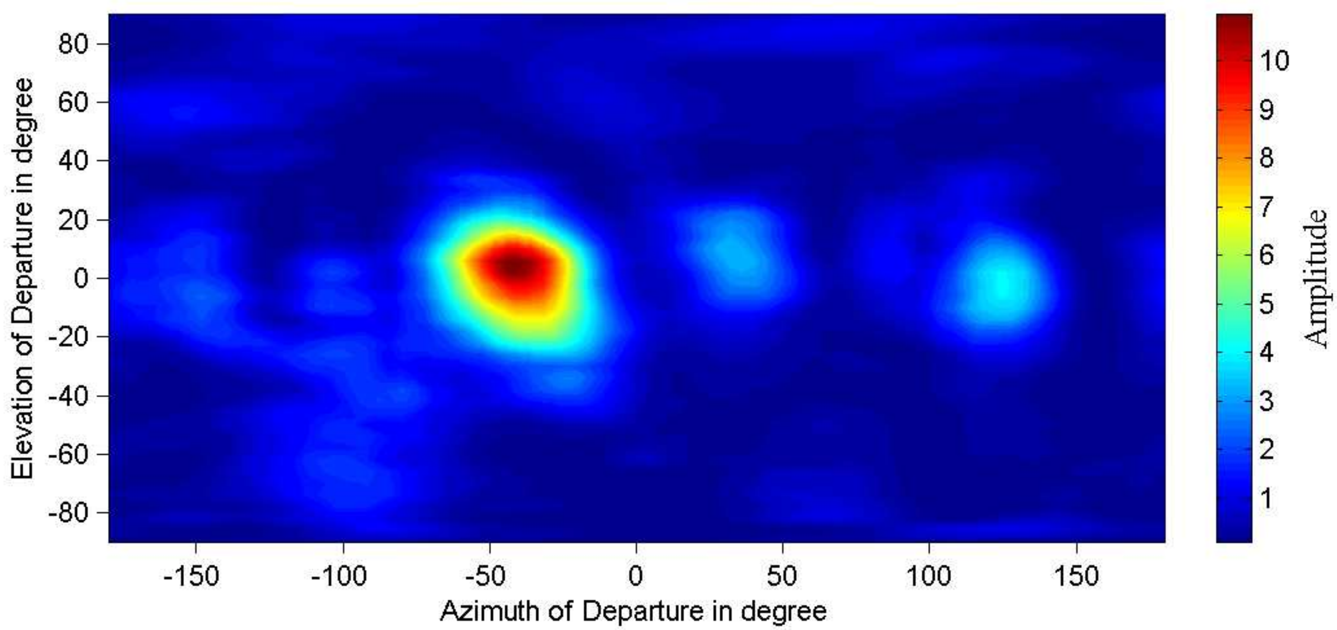

An experimental example: direction and delay dispersion of an indoor propagation channel

- Average delay power spectrum

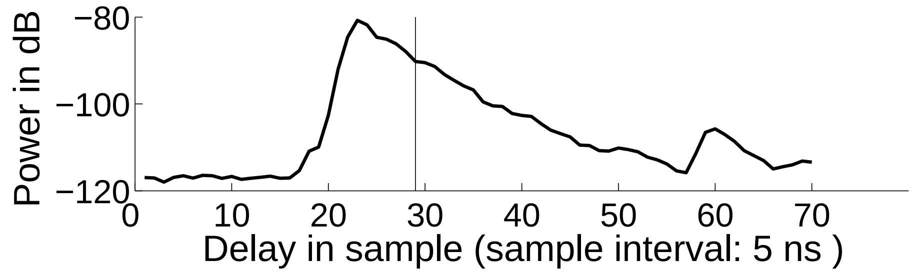

- Bartlett spectrum w.r.t. azimuth and elevation of departure at delay 145 ns:

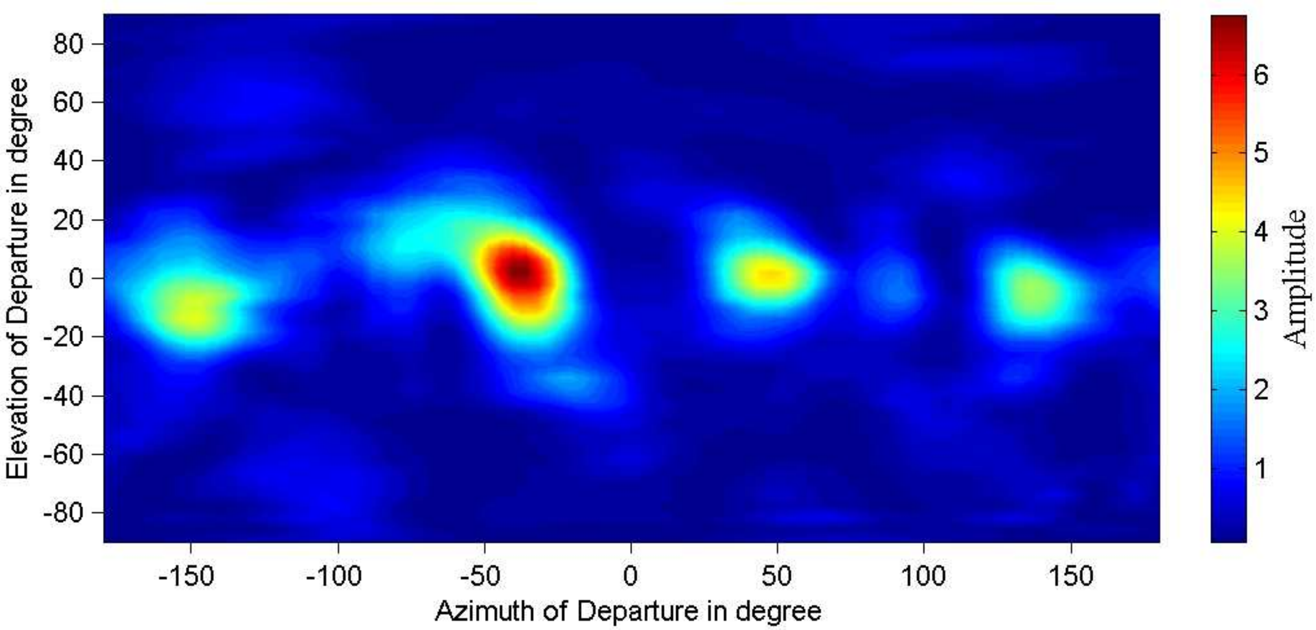

An experimental example: direction and delay dispersion of an indoor propagation channel

- Average delay power spectrum

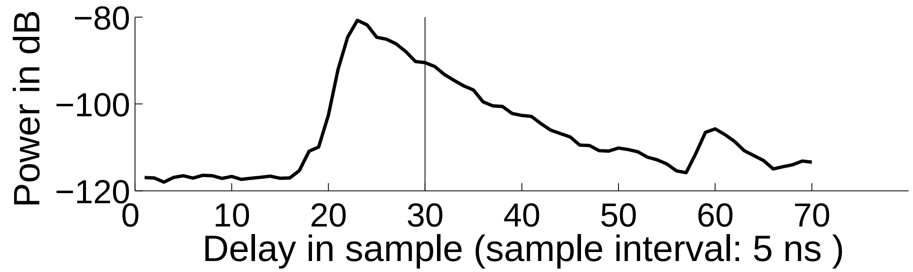

- Bartlett spectrum w.r.t. azimuth and elevation of departure at delay 150 ns:

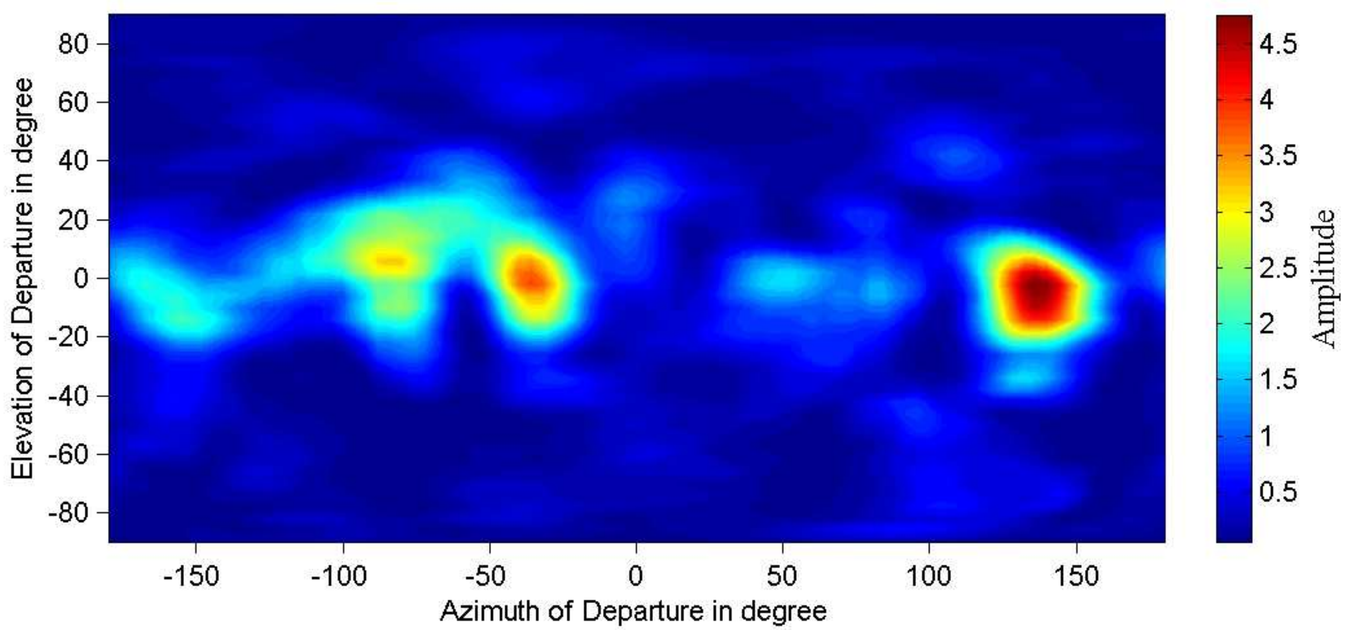

An experimental example: direction and delay dispersion of an indoor propagation channel

- Average delay power spectrum

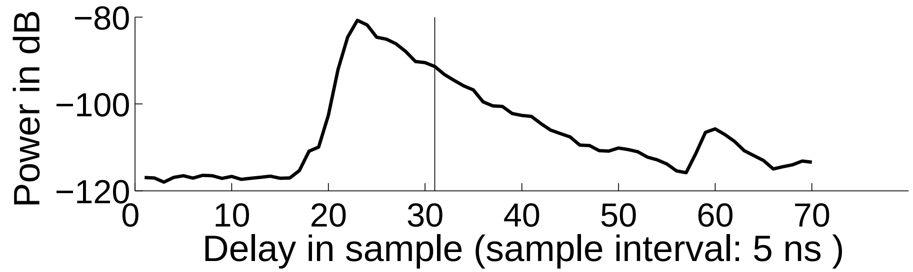

- Bartlett spectrum w.r.t. azimuth and elevation of departure at delay 155 ns:

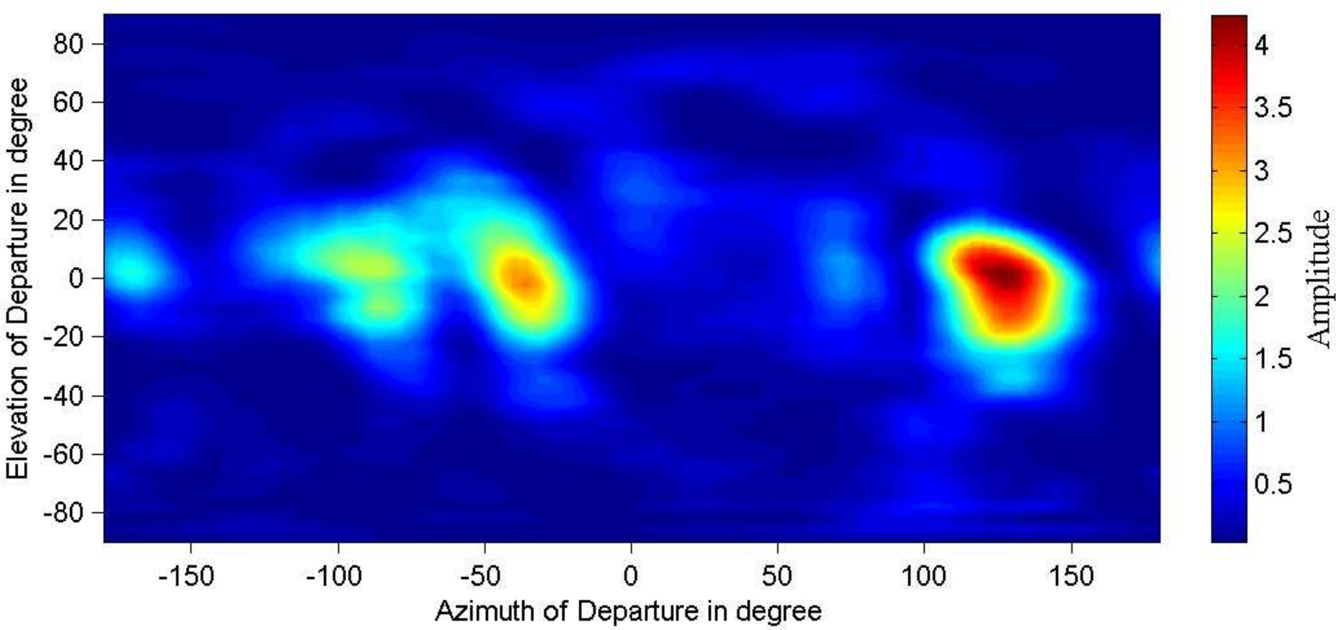

An experimental example: direction and delay dispersion of an indoor propagation channel

- Average delay power spectrum

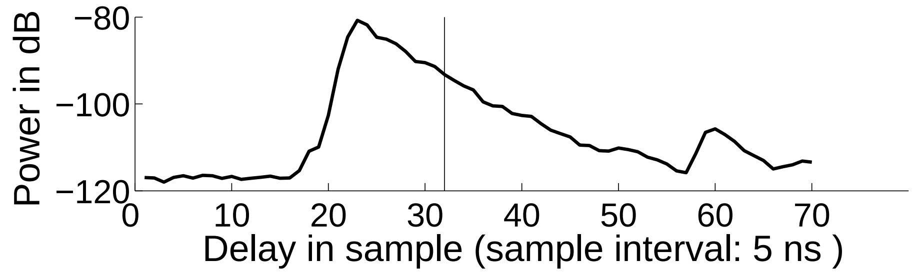

- Bartlett spectrum w.r.t. azimuth and elevation of departure at delay 160 ns:

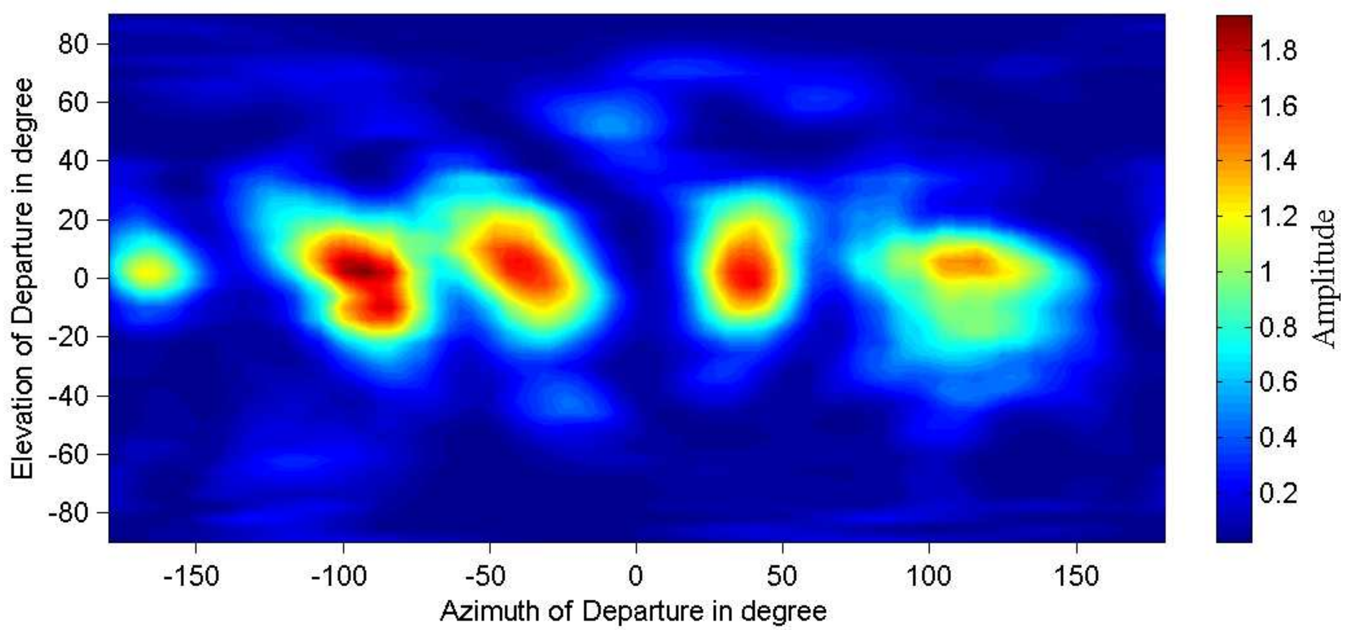

An experimental example: direction and delay dispersion of an indoor propagation channel

- Average delay power spectrum

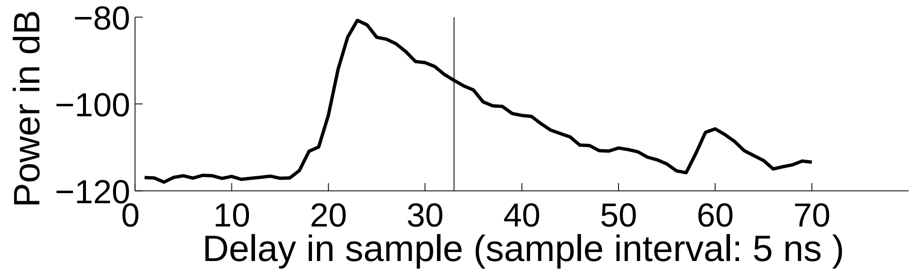

- Bartlett spectrum w.r.t. azimuth and elevation of departure at delay 165 ns:

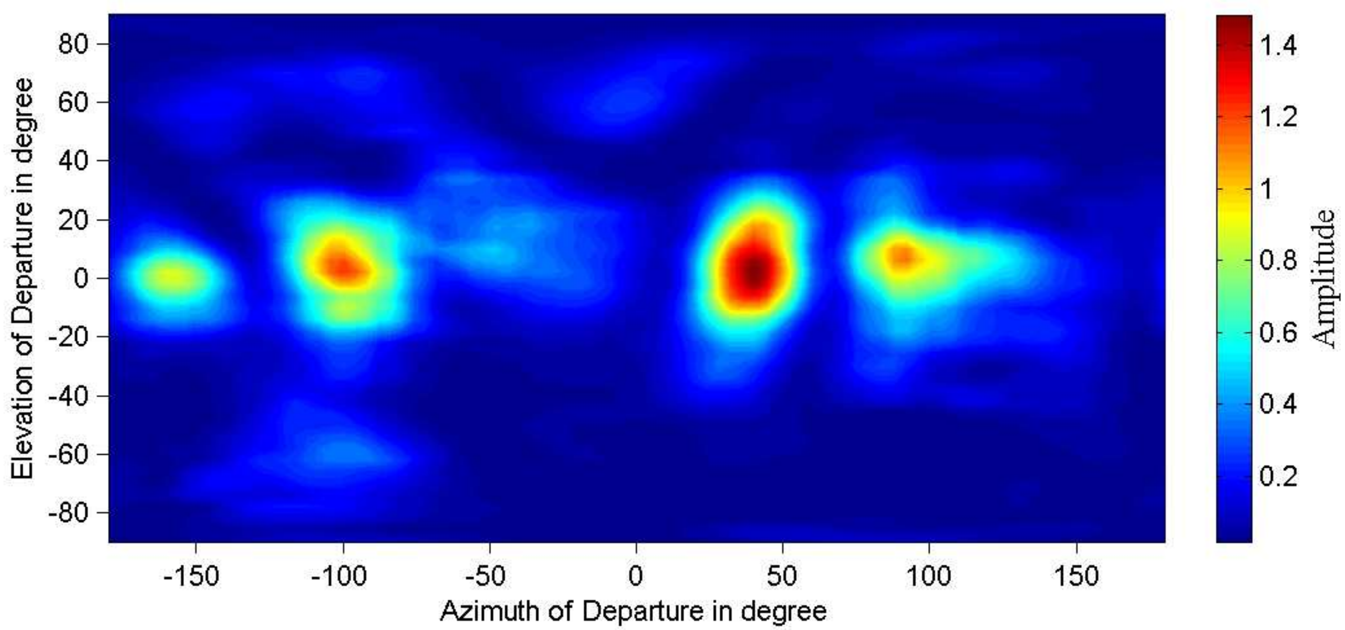

An experimental example: direction and delay dispersion of an indoor propagation channel

- Average delay power spectrum

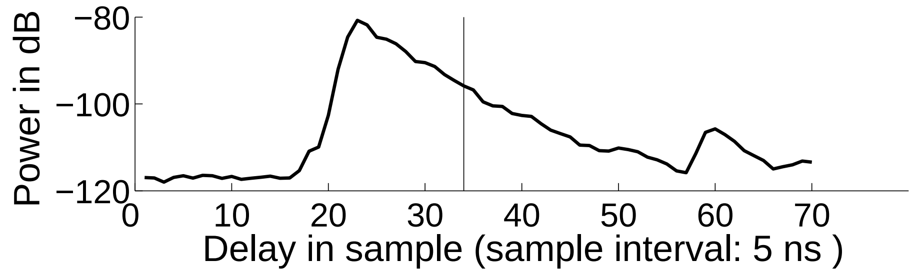

- Bartlett spectrum w.r.t. azimuth and elevation of departure at delay 170 ns:

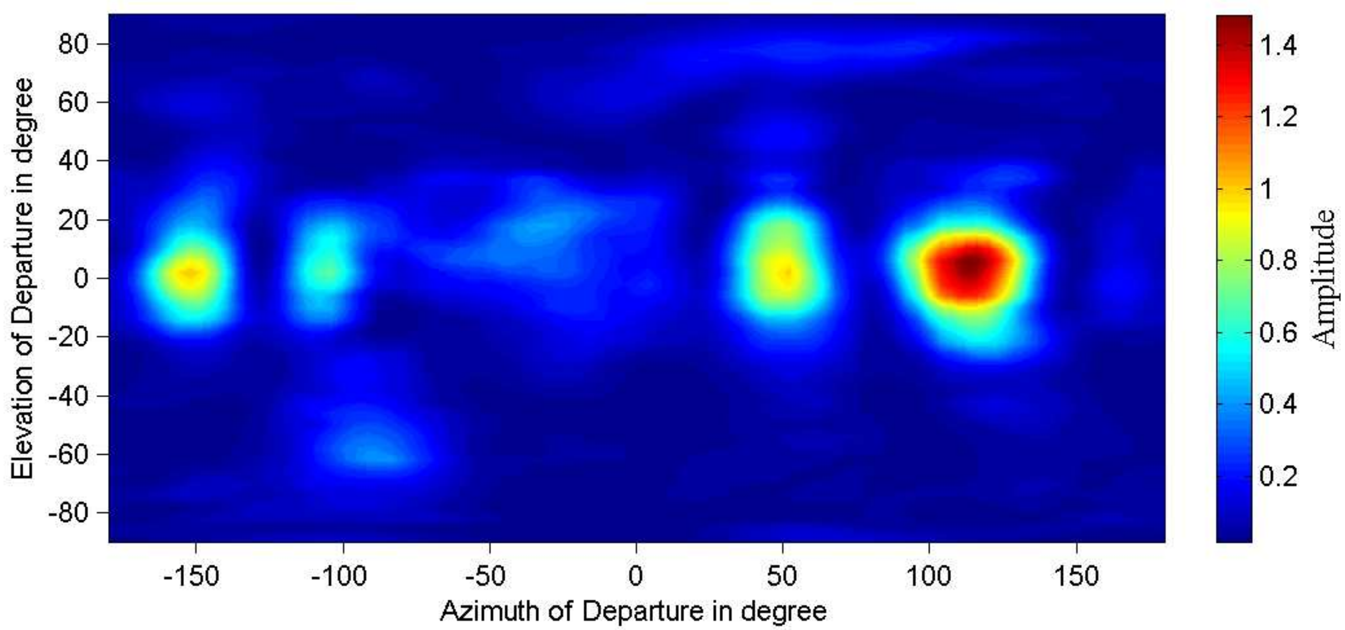

An experimental example: direction and delay dispersion of an indoor propagation channel

- Average delay power spectrum

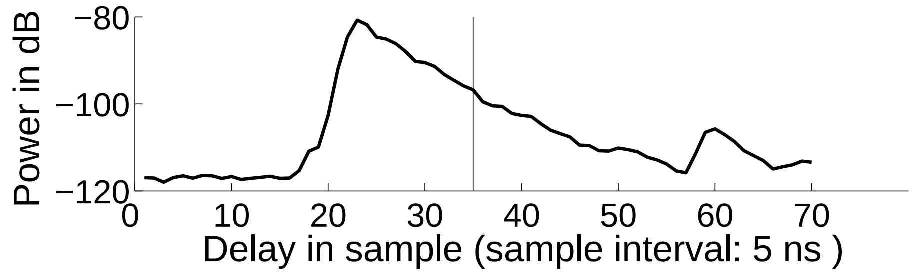

- Bartlett spectrum w.r.t. azimuth and elevation of departure at delay 175 ns:

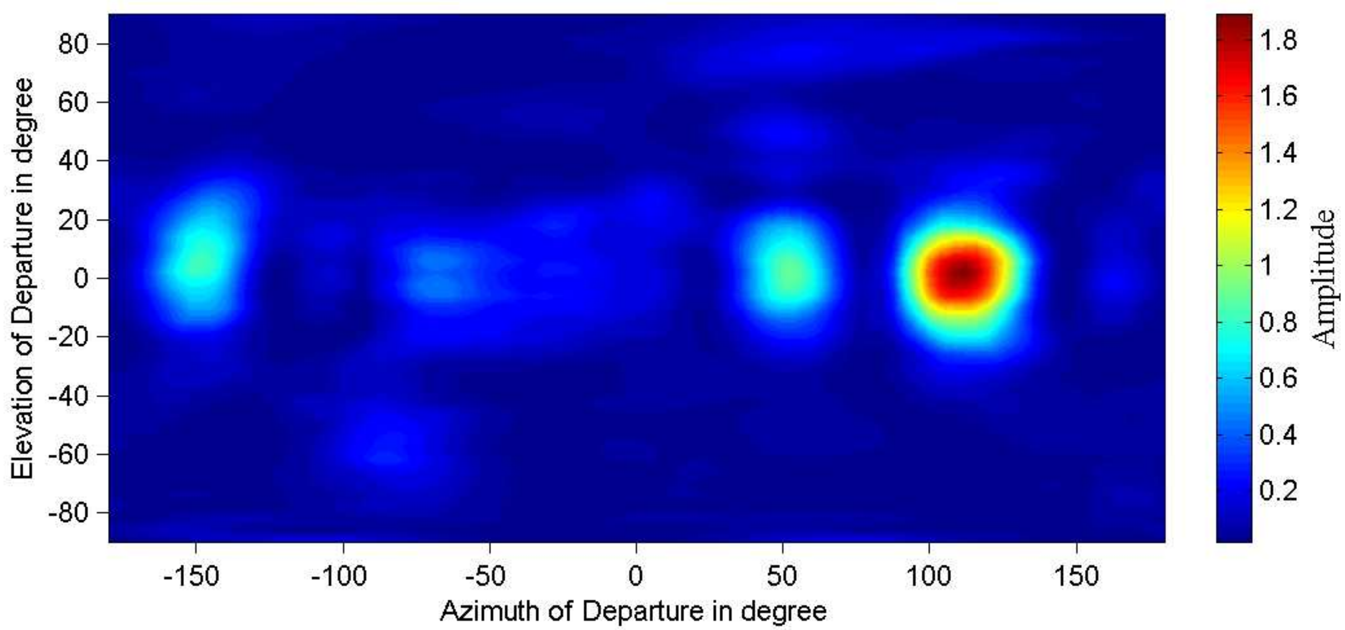

An experimental example: direction and delay dispersion of an indoor propagation channel

- Average delay power spectrum

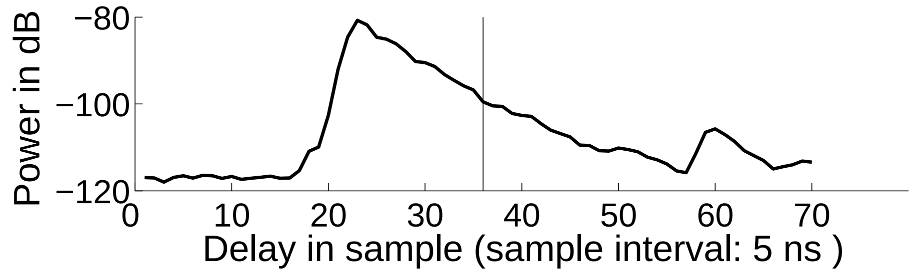

- Bartlett spectrum w.r.t. azimuth and elevation of departure at delay 180 ns:

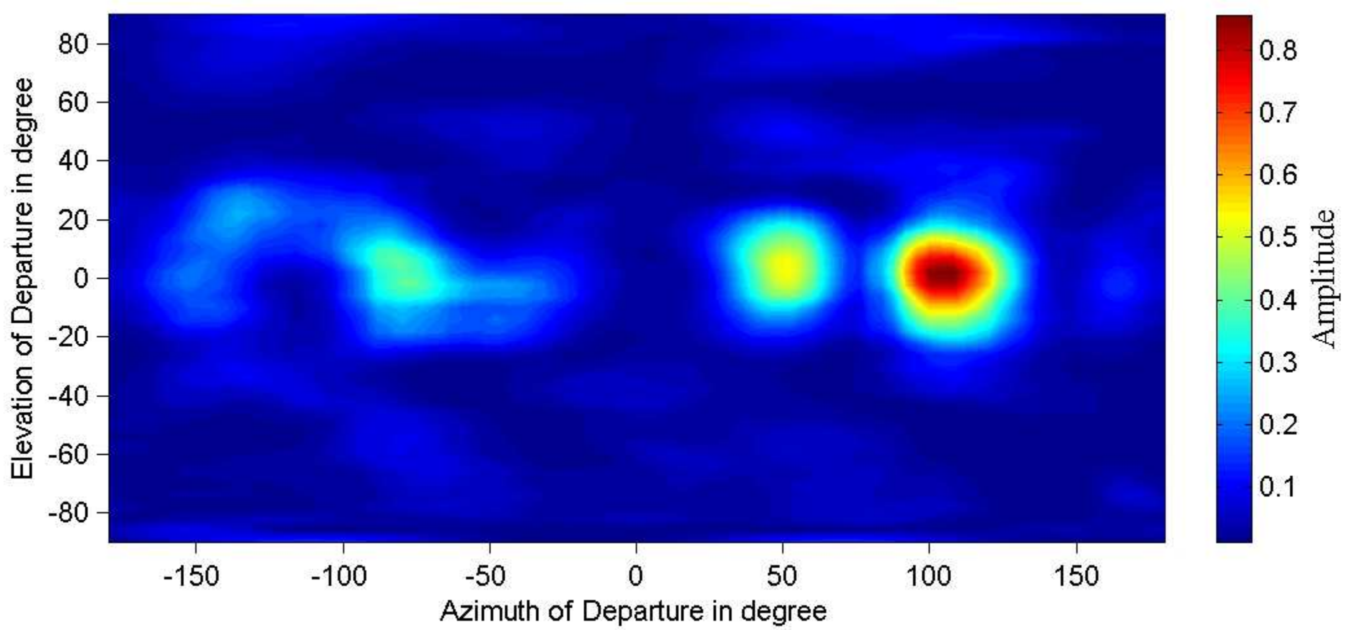

An experimental example: direction and delay dispersion of an indoor propagation channel

- Average delay power spectrum

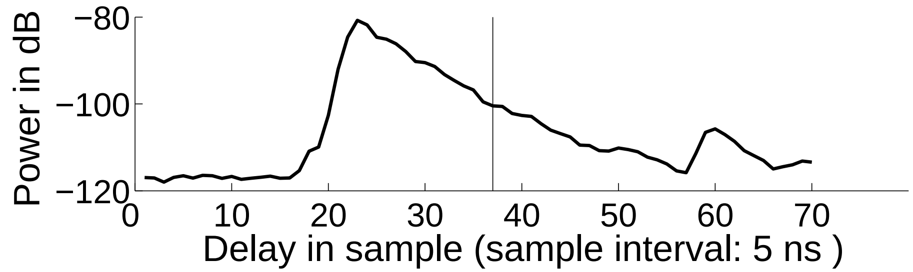

- Bartlett spectrum w.r.t. azimuth and elevation of departure at delay 185 ns:

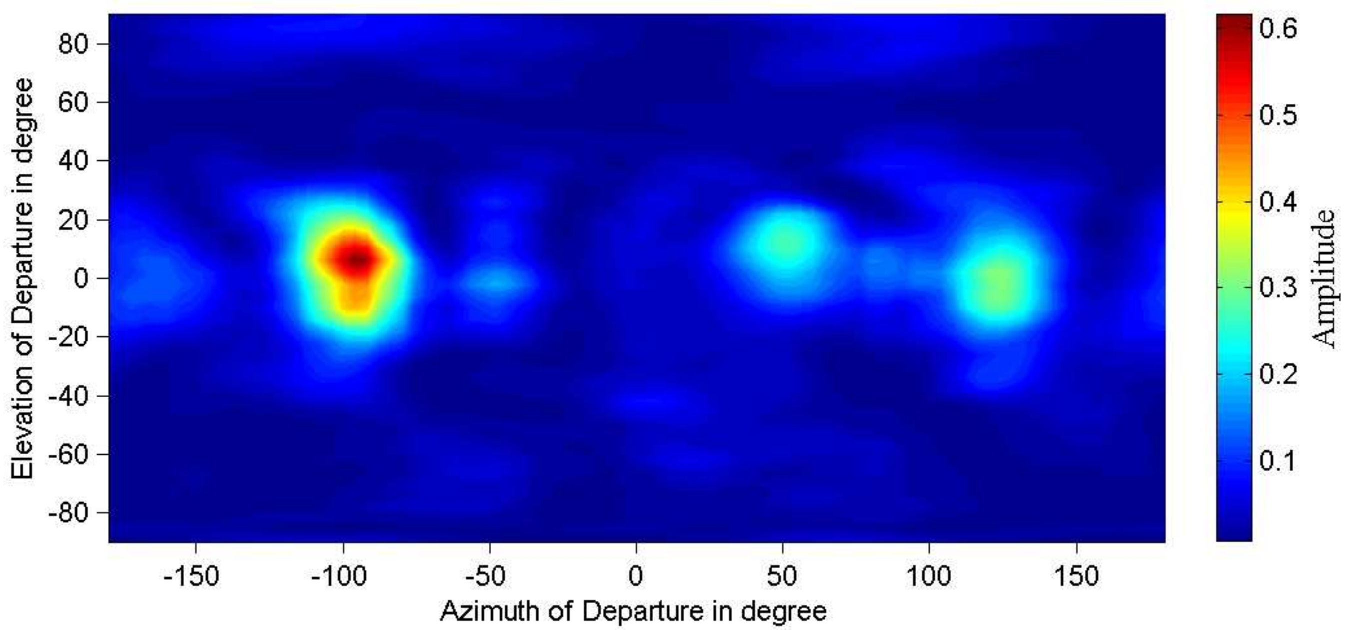

An experimental example: direction and delay dispersion of an indoor propagation channel

- Average delay power spectrum

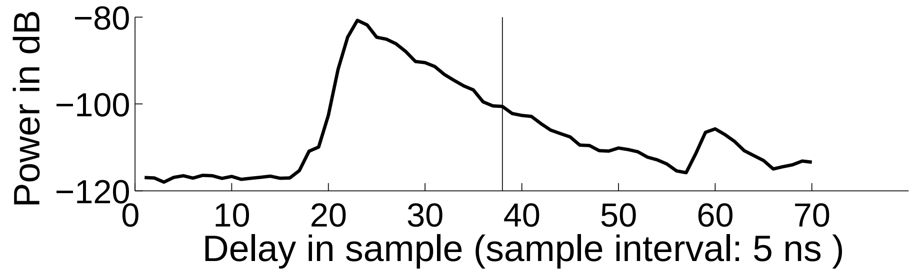

- Bartlett spectrum w.r.t. azimuth and elevation of departure at delay 100 ns:

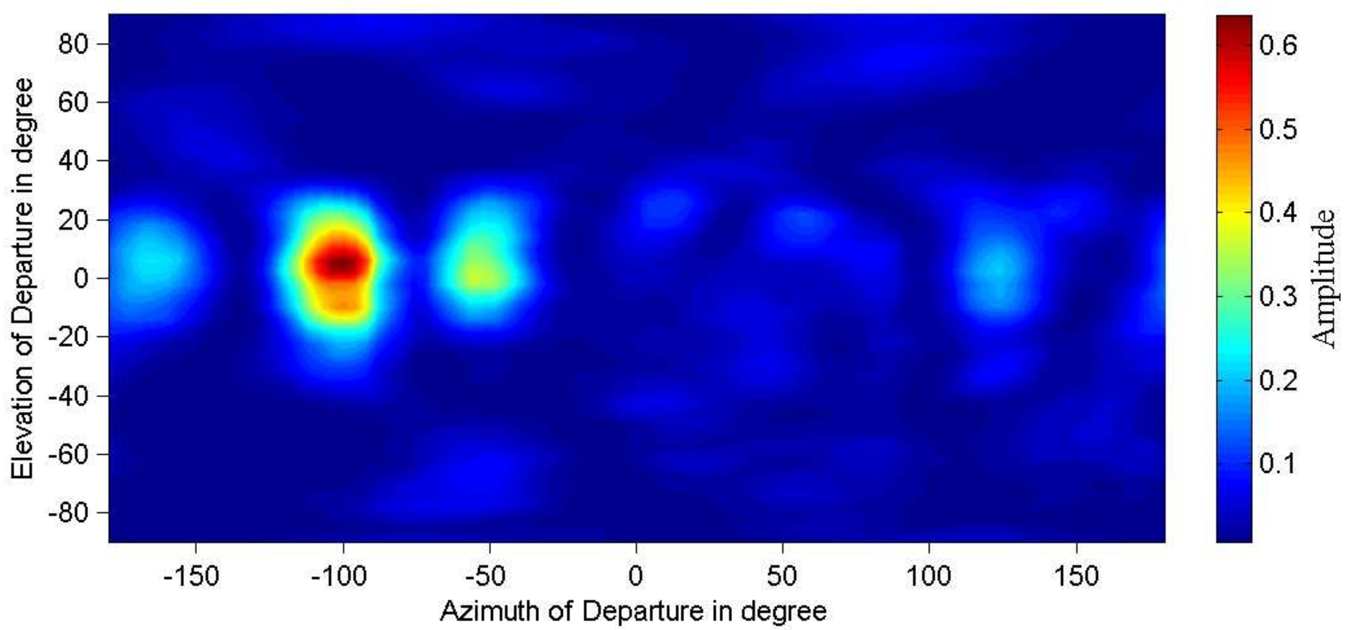

An experimental example: direction and delay dispersion of an indoor propagation channel

- Average delay power spectrum

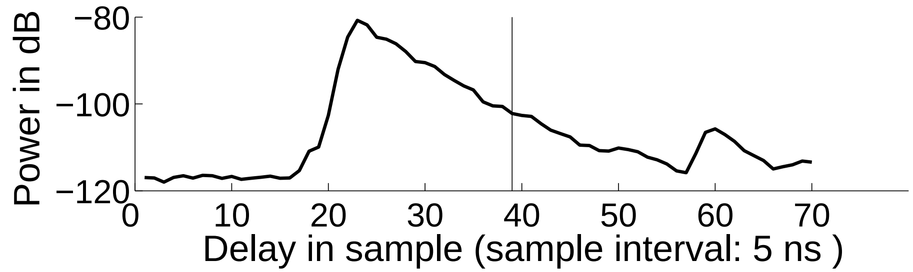

- Bartlett spectrum w.r.t. azimuth and elevation of departure at delay 105 ns:

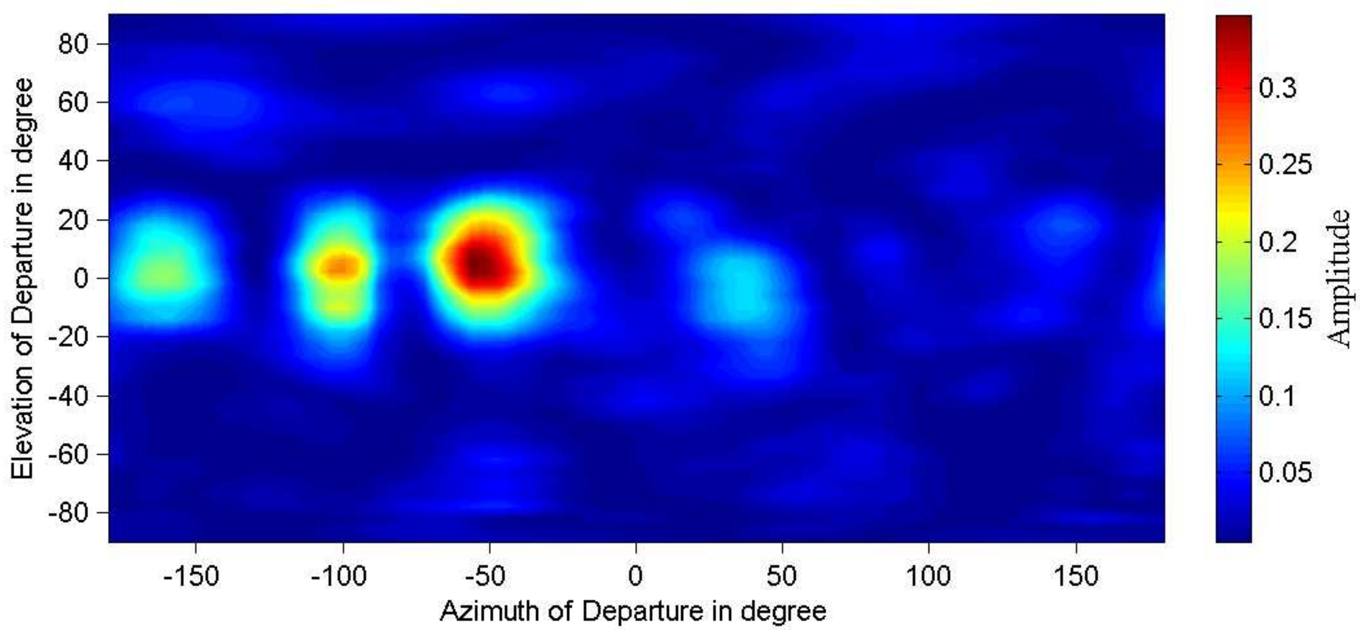

An experimental example: direction and delay dispersion of an indoor propagation channel

- Average delay power spectrum

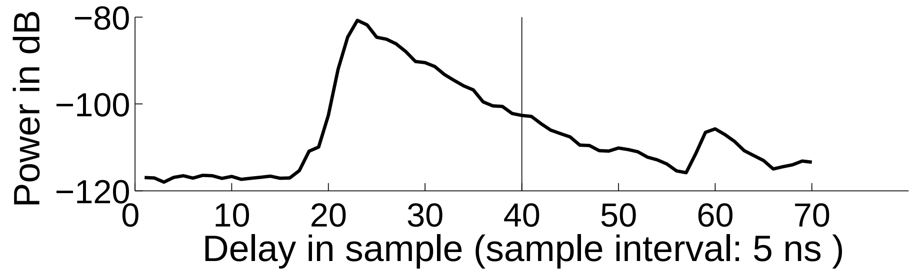

- Bartlett spectrum w.r.t. azimuth and elevation of departure at delay 200 ns:

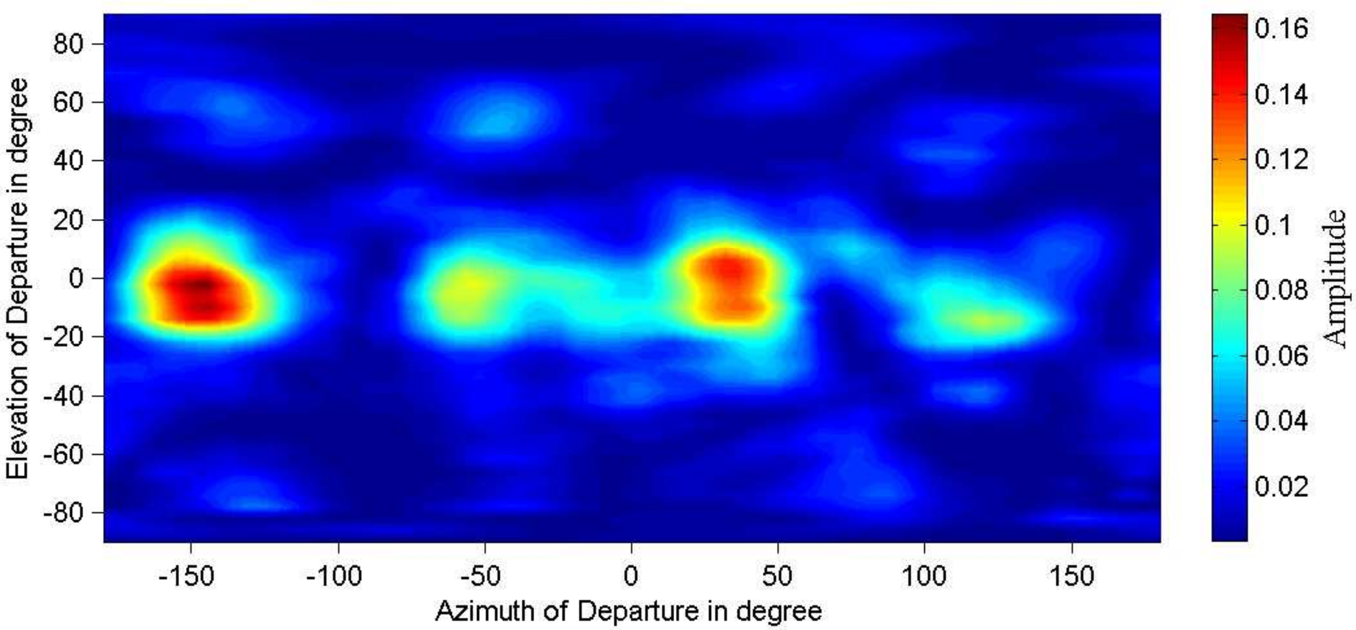

An experimental example: direction and delay dispersion of an indoor propagation channel

- Average delay power spectrum

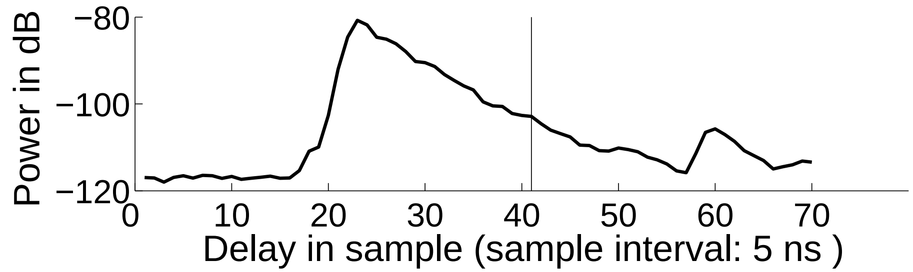

- Bartlett spectrum w.r.t. azimuth and elevation of departure at delay 205 ns:

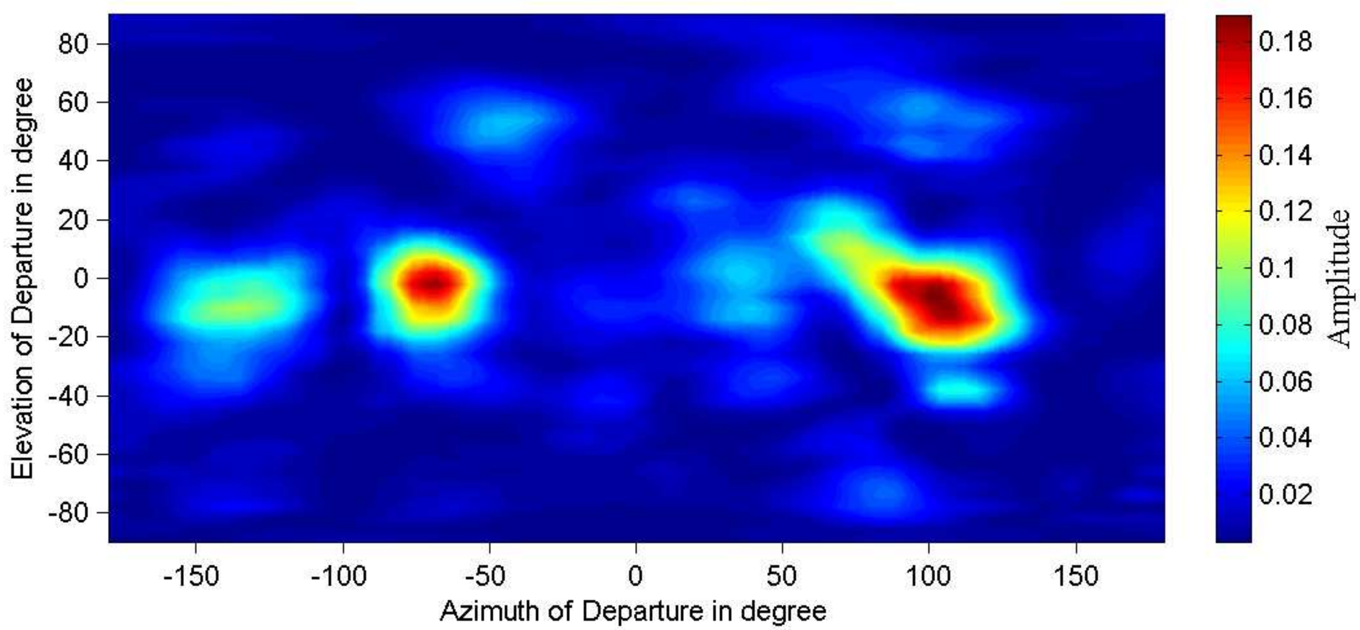

An experimental example: direction and delay dispersion of an indoor propagation channel

- Average delay power spectrum

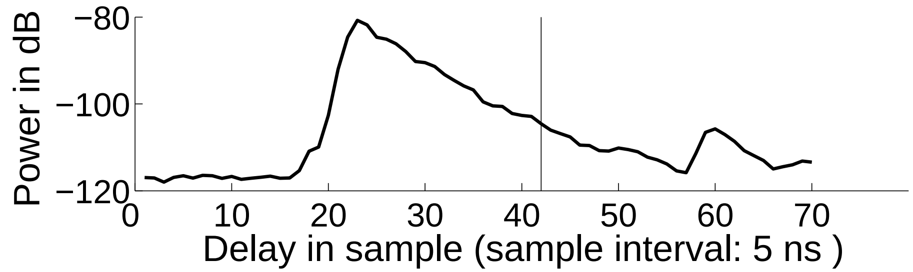

- Bartlett spectrum w.r.t. azimuth and elevation of departure at delay 210 ns:

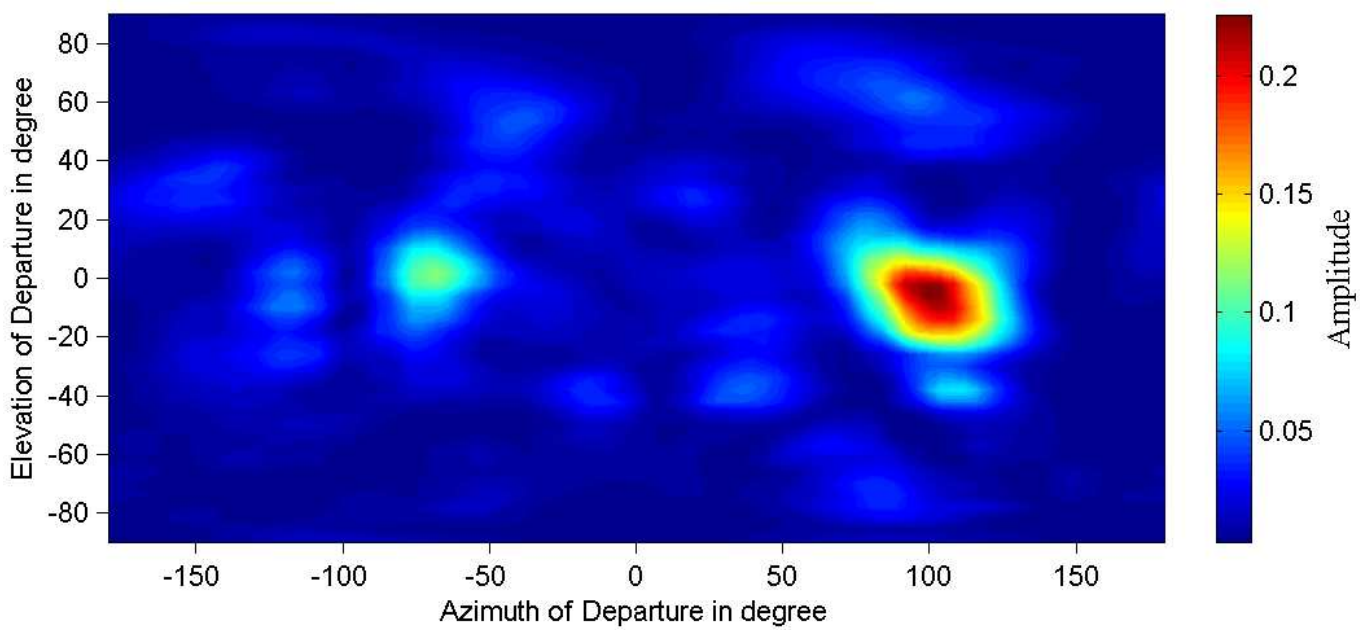

An experimental example: direction and delay dispersion of an indoor propagation channel

- Average delay power spectrum

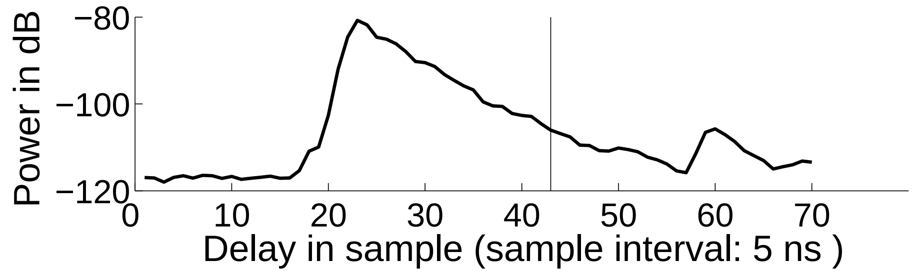

- Bartlett spectrum w.r.t. azimuth and elevation of departure at delay 215 ns:

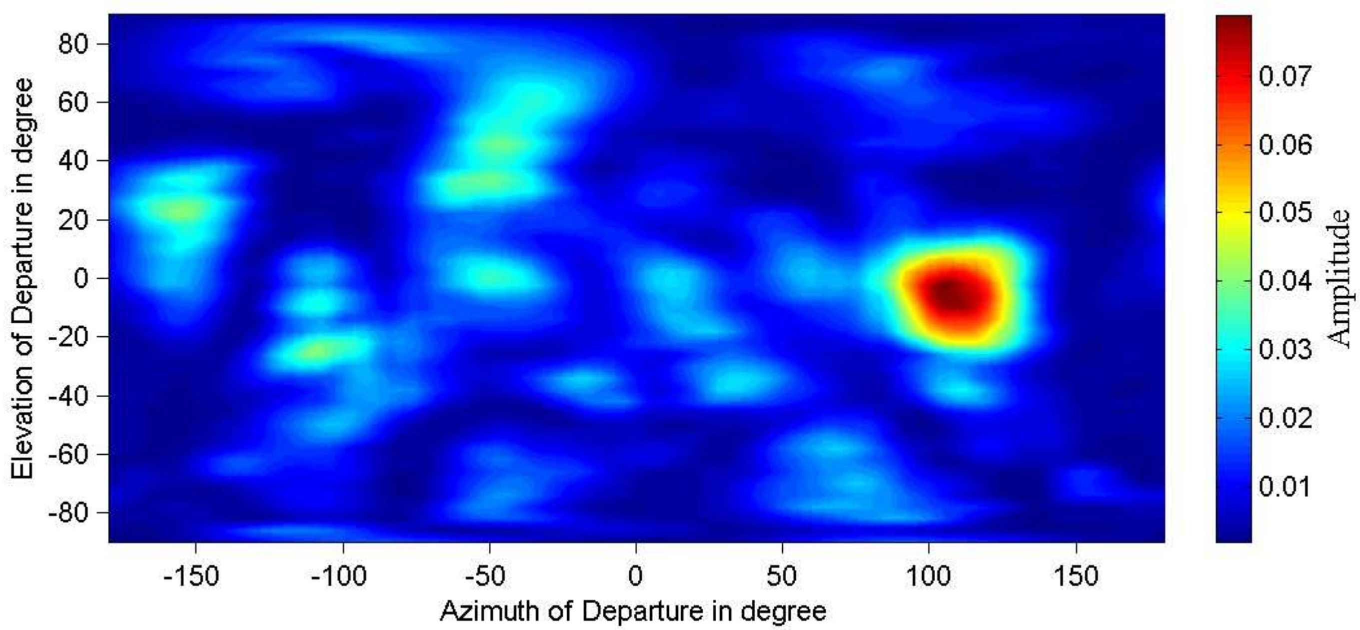

An experimental example: direction and delay dispersion of an indoor propagation channel

- Average delay power spectrum

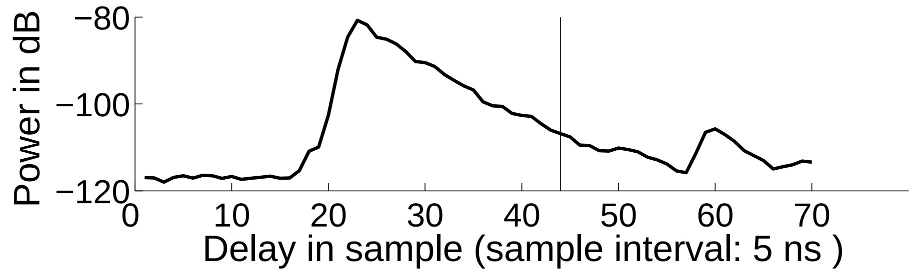

- Bartlett spectrum w.r.t. azimuth and elevation of departure at delay 220 ns:

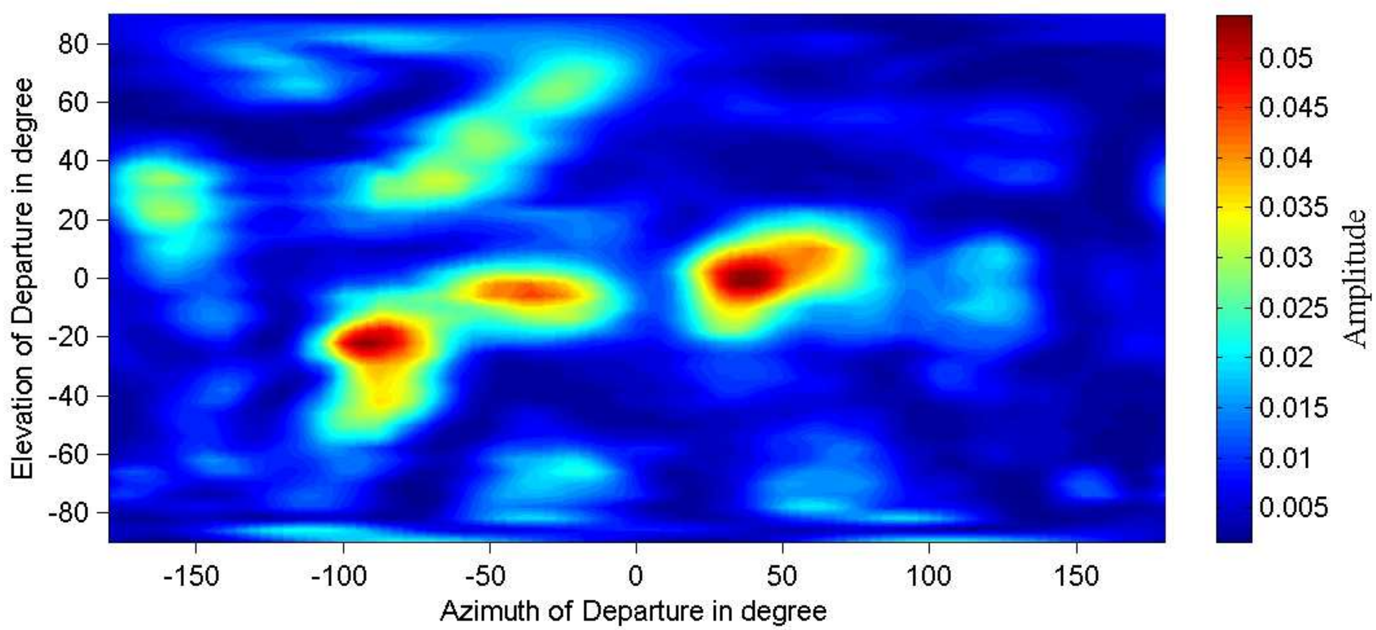

An experimental example: direction and delay dispersion of an indoor propagation channel

- Average delay power spectrum

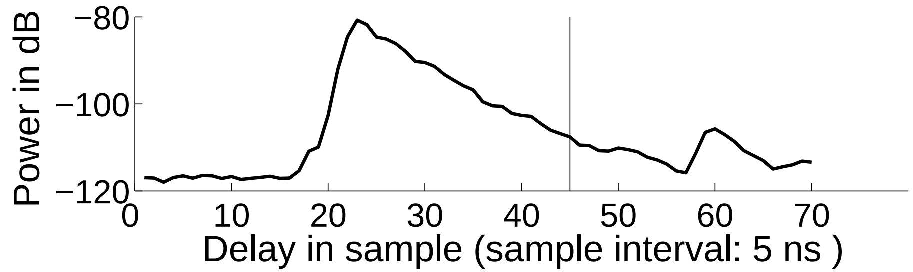

- Bartlett spectrum w.r.t. azimuth and elevation of departure at delay 225 ns:

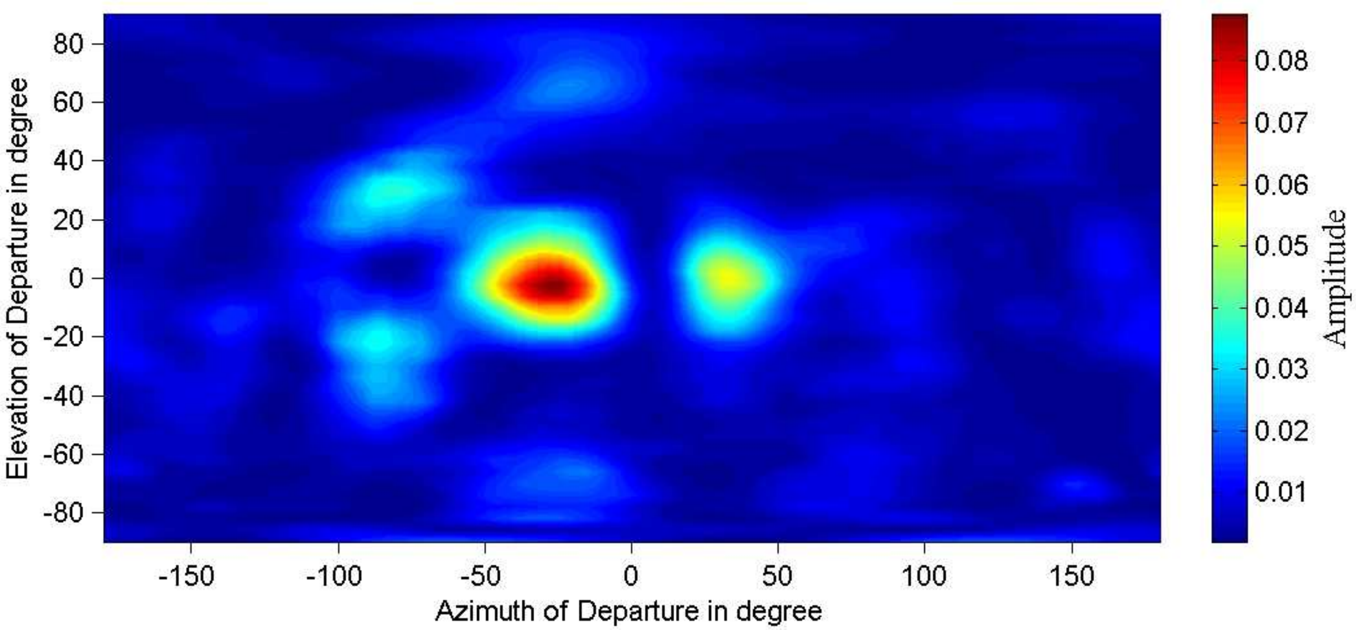

An experimental example: direction and delay dispersion of an indoor propagation channel

- Average delay power spectrum

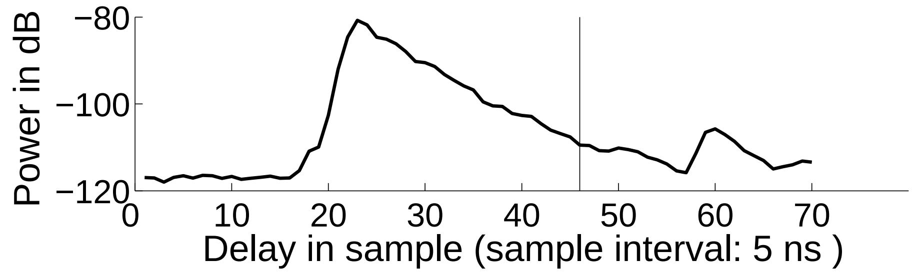

- Bartlett spectrum w.r.t. azimuth and elevation of departure at delay 230 ns:

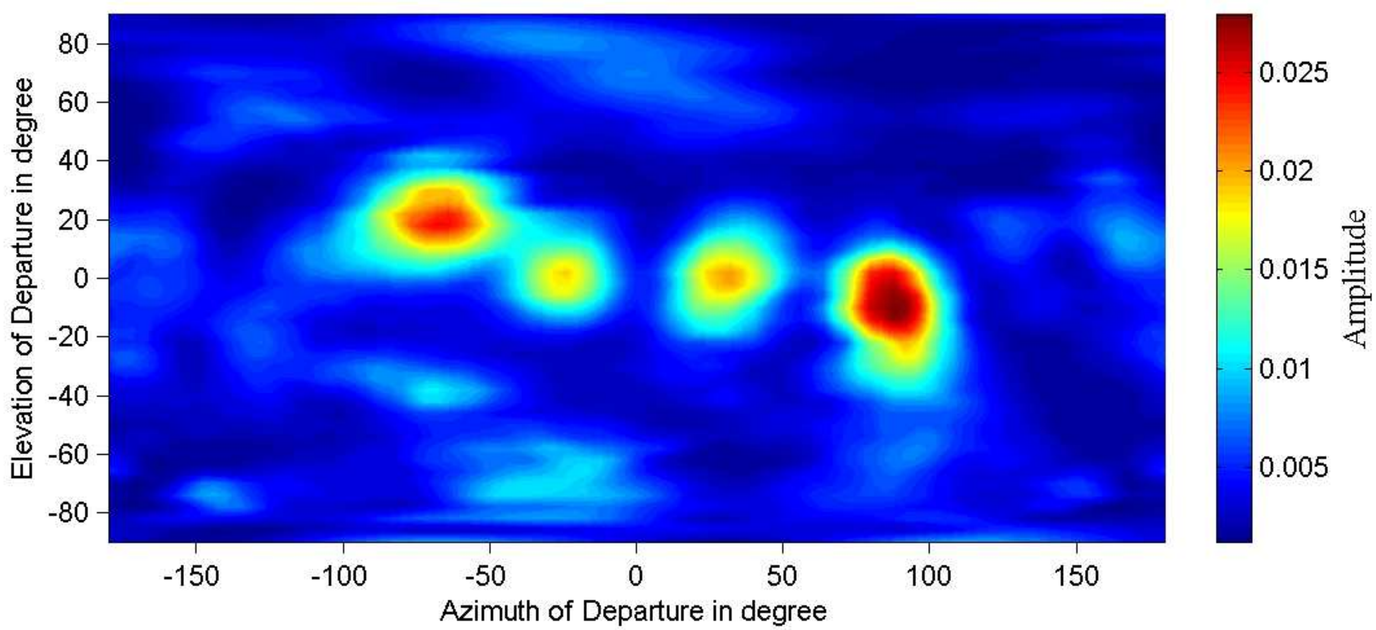

An experimental example: direction and delay dispersion of an indoor propagation channel

- Average delay power spectrum

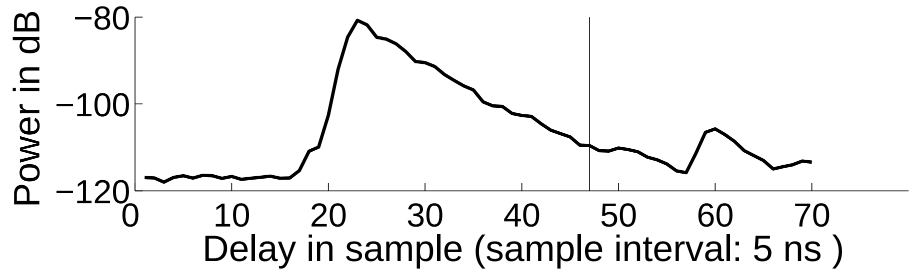

- Bartlett spectrum w.r.t. azimuth and elevation of departure at delay 235 ns:

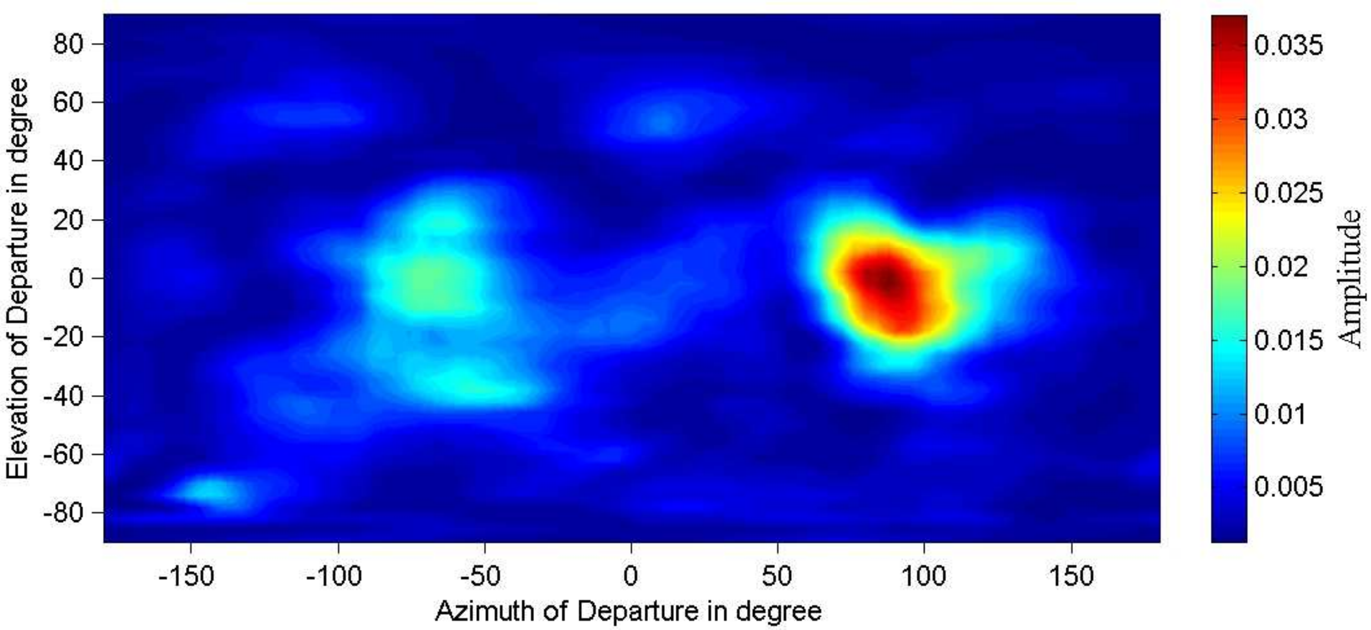

An experimental example: direction and delay dispersion of an indoor propagation channel

- Average delay power spectrum

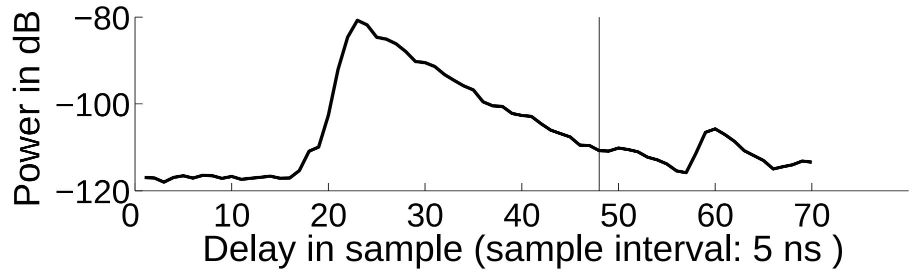

- Bartlett spectrum w.r.t. azimuth and elevation of departure at delay 240 ns:

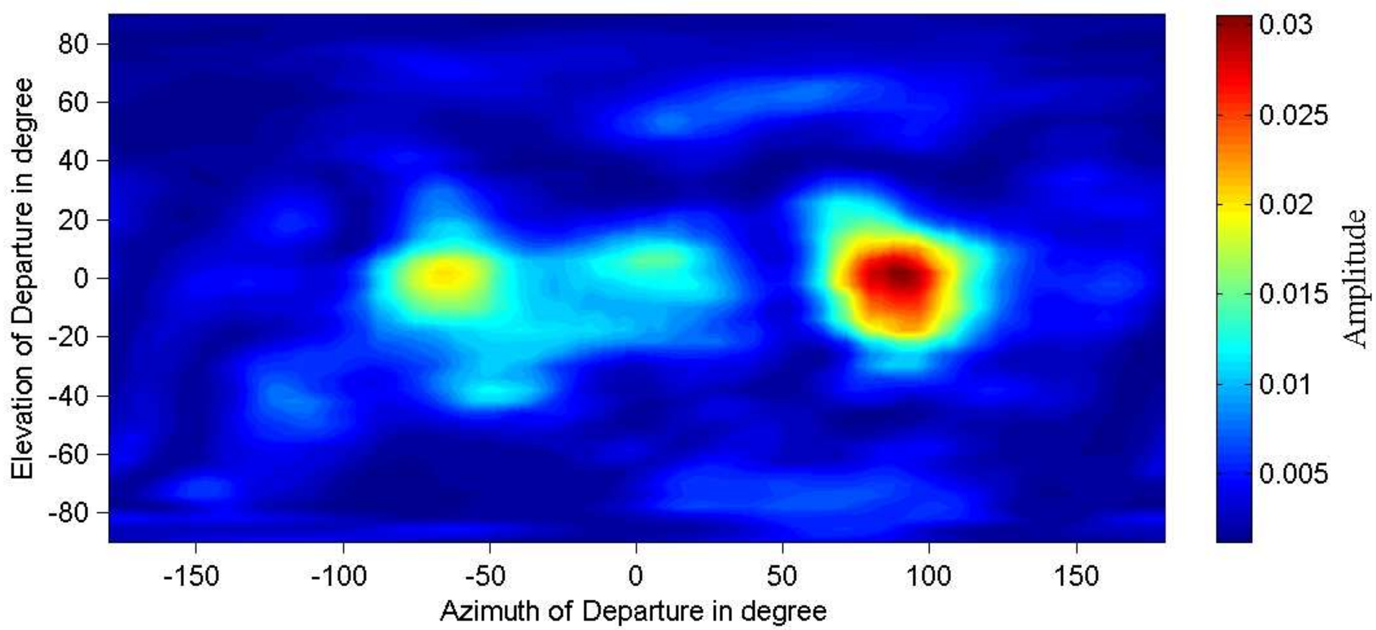

An experimental example: direction and delay dispersion of an indoor propagation channel

- Average delay power spectrum

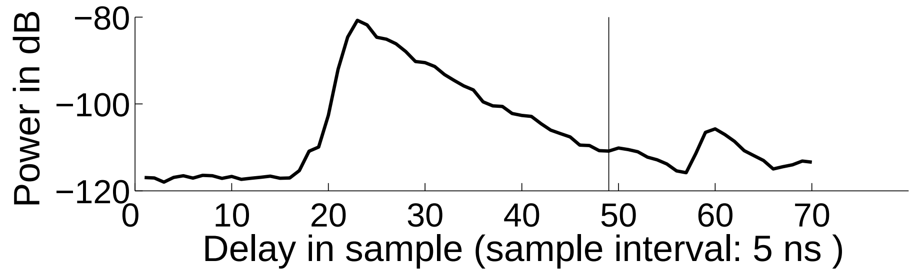

- Bartlett spectrum w.r.t. azimuth and elevation of departure at delay 245 ns:

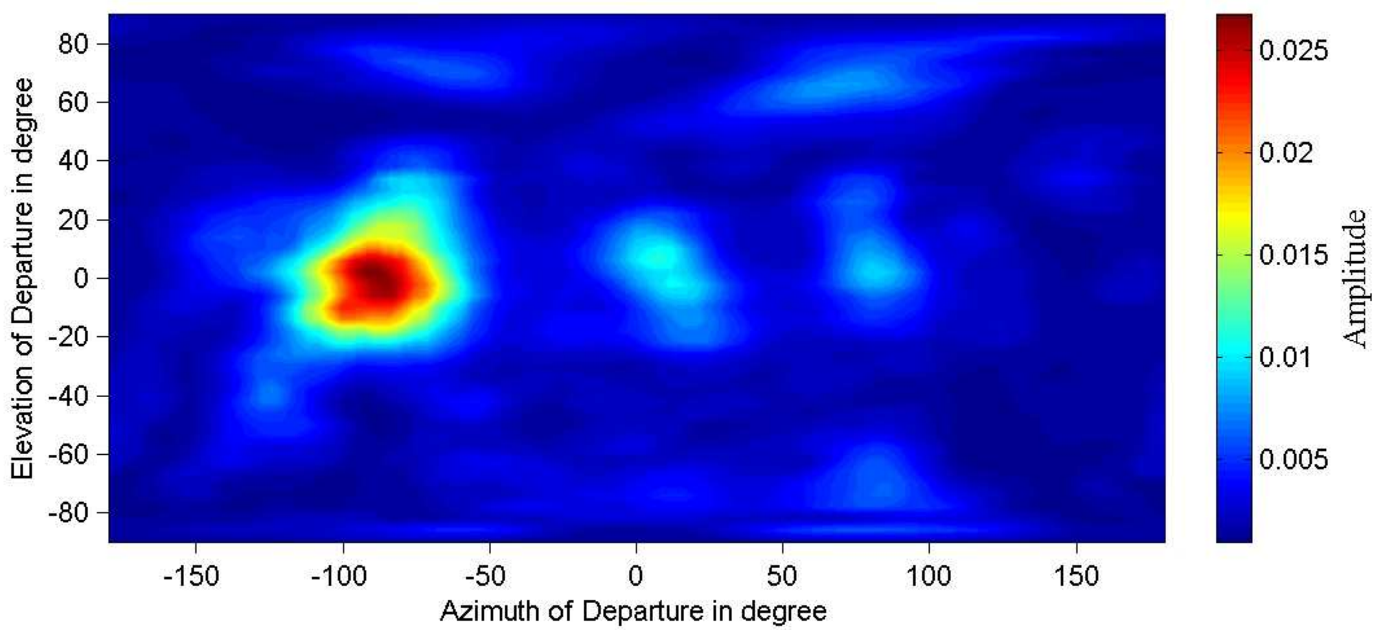

An experimental example: direction and delay dispersion of an indoor propagation channel

- Average delay power spectrum

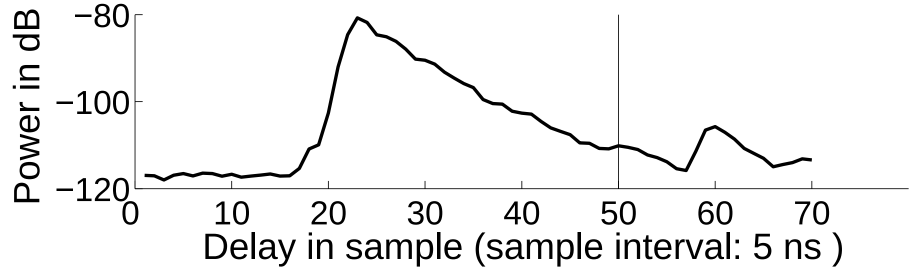

- Bartlett spectrum w.r.t. azimuth and elevation of departure at delay 250 ns:

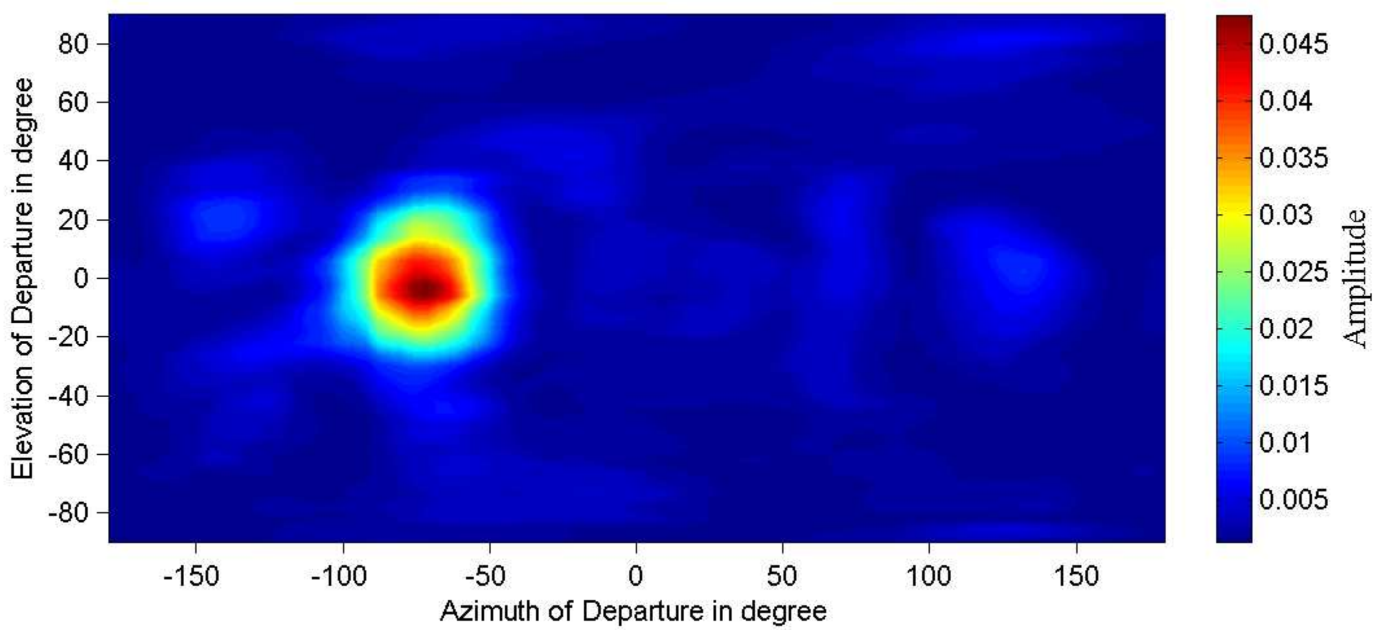

An experimental example: direction and delay dispersion of an indoor propagation channel

- Average delay power spectrum

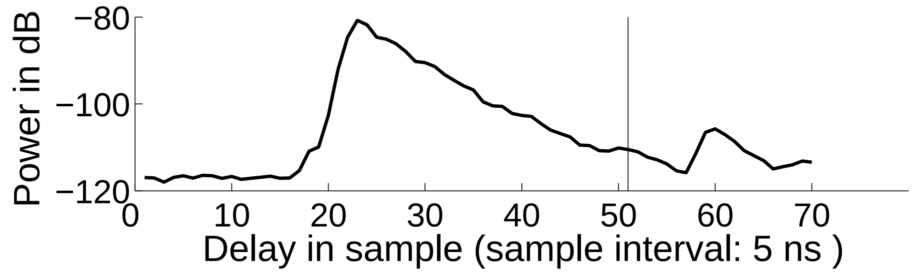

- Bartlett spectrum w.r.t. azimuth and elevation of departure at delay 255 ns:

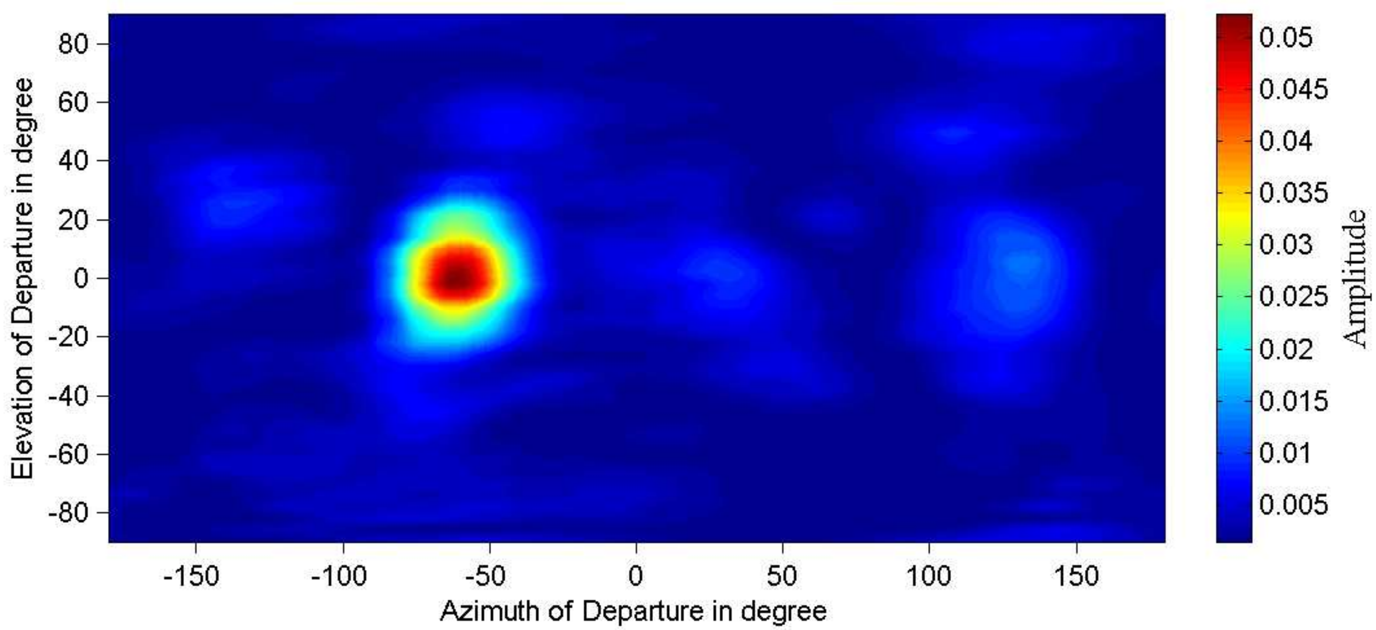

An experimental example: direction and delay dispersion of an indoor propagation channel

- Average delay power spectrum

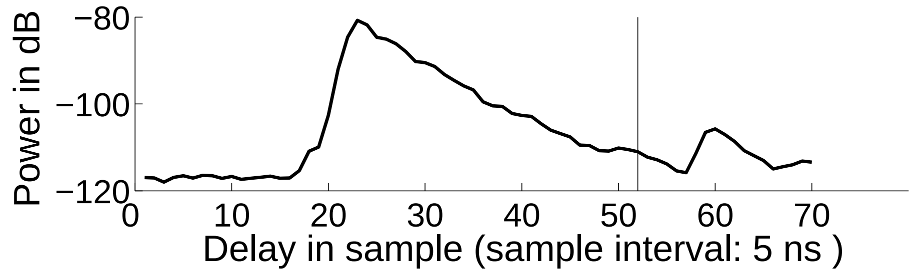

- Bartlett spectrum w.r.t. azimuth and elevation of departure at delay 260 ns:

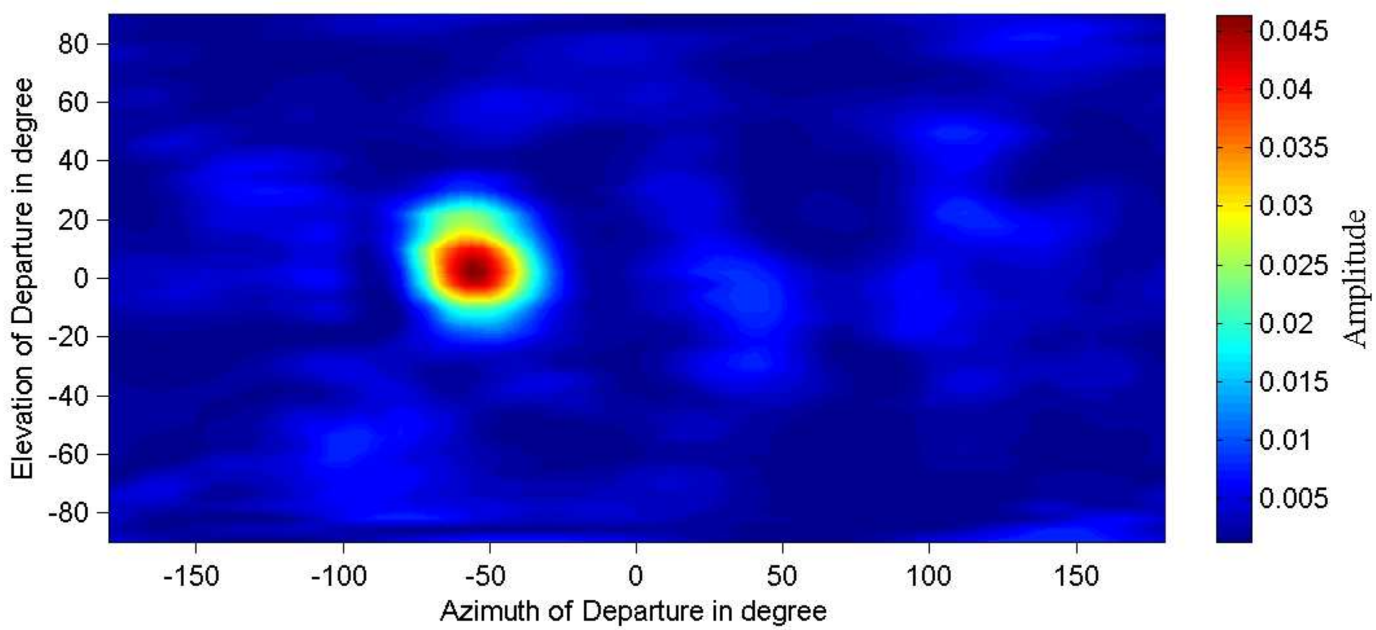

An experimental example: direction and delay dispersion of an indoor propagation channel

- Average delay power spectrum

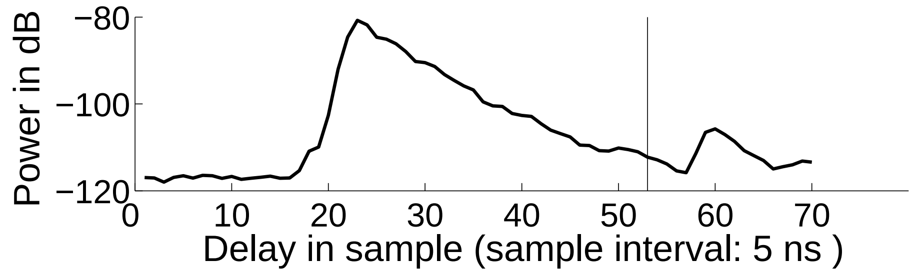

- Bartlett spectrum w.r.t. azimuth and elevation of departure at delay 265 ns:

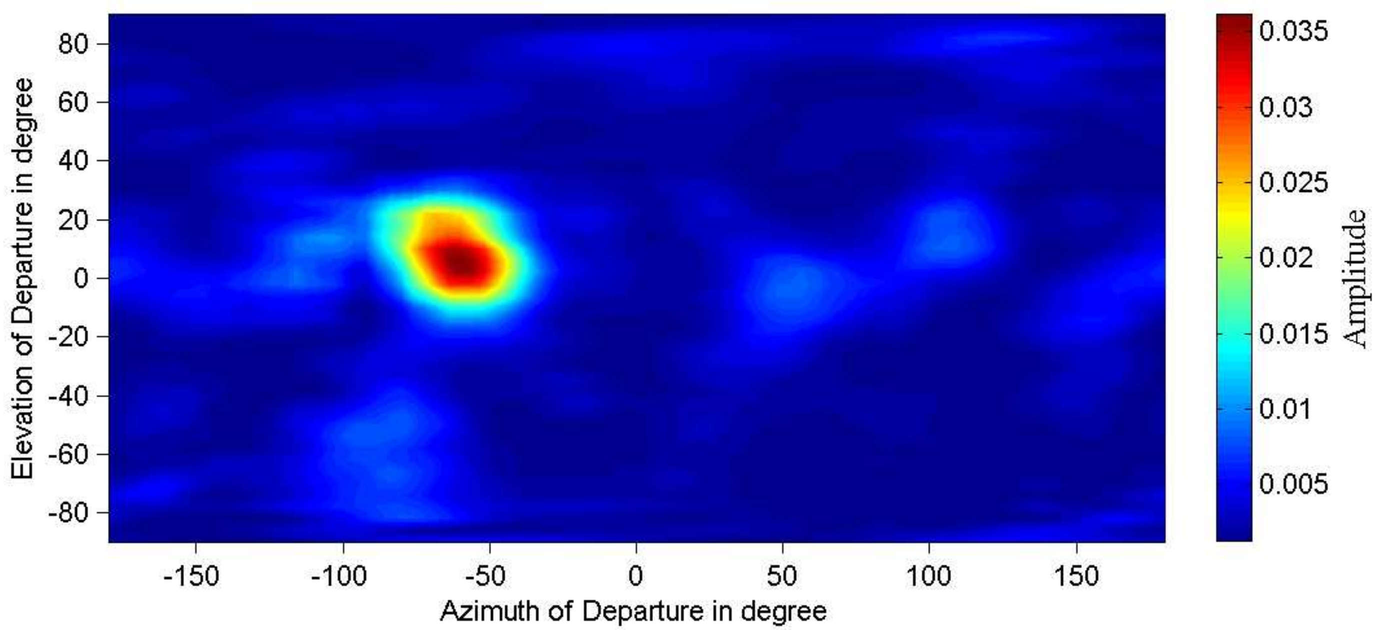

An experimental example: direction and delay dispersion of an indoor propagation channel

- Average delay power spectrum

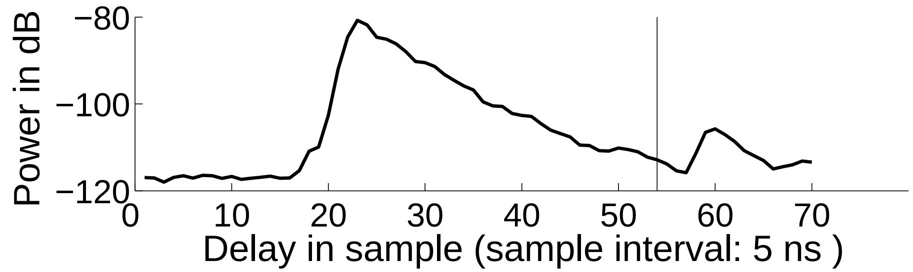

- Bartlett spectrum w.r.t. azimuth and elevation of departure at delay 270 ns:

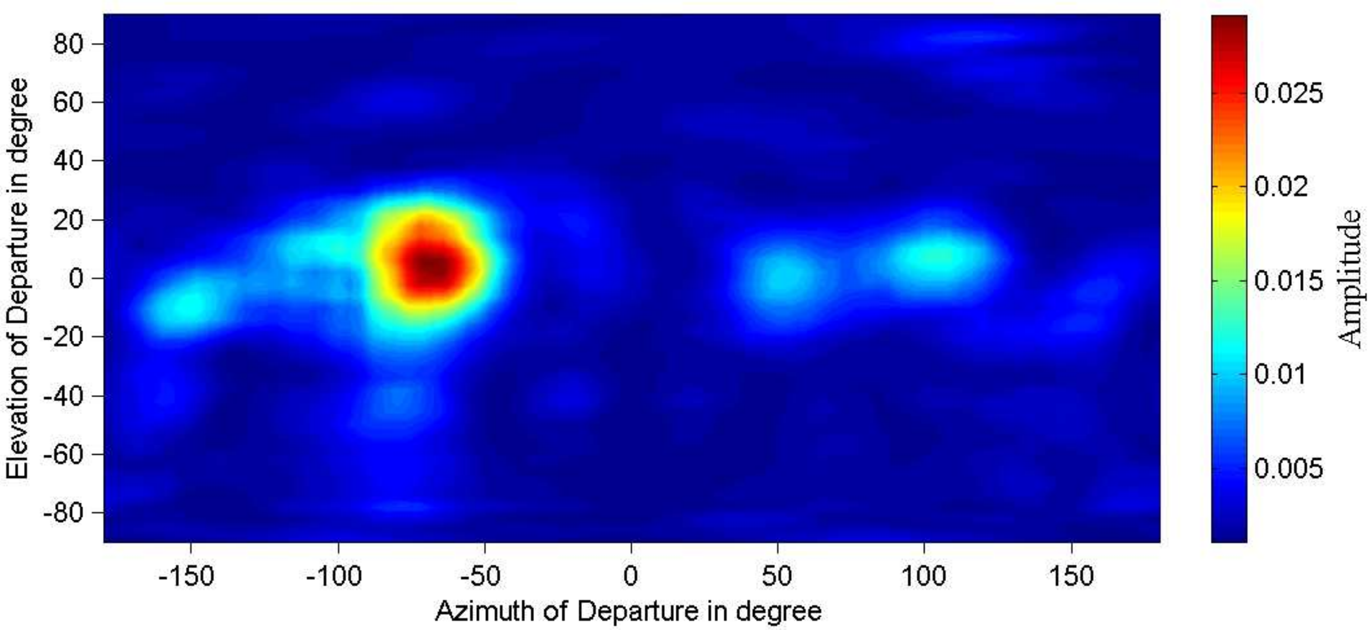

An experimental example: direction and delay dispersion of an indoor propagation channel

- Average delay power spectrum

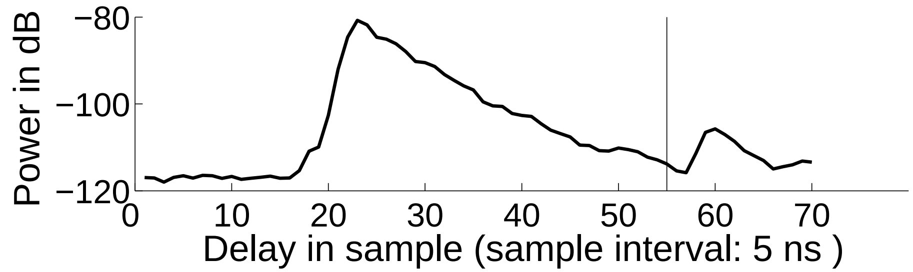

- Bartlett spectrum w.r.t. azimuth and elevation of departure at delay 275 ns:

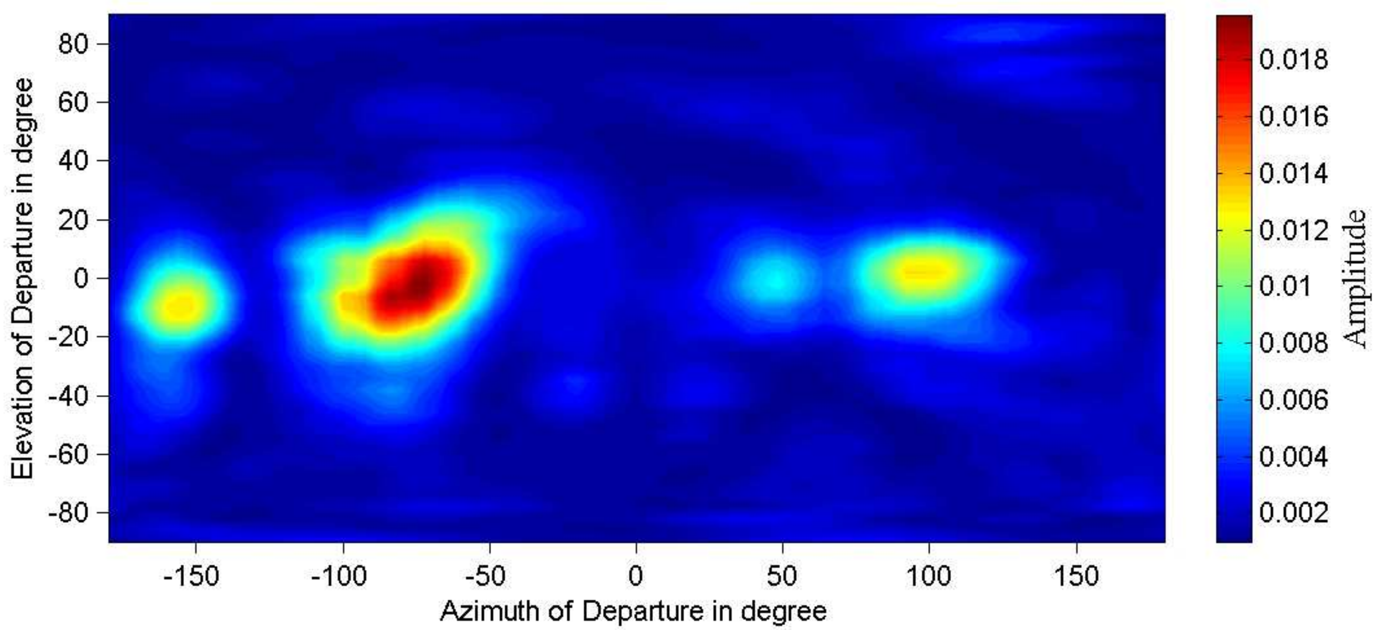

An experimental example: direction and delay dispersion of an indoor propagation channel

- Average delay power spectrum

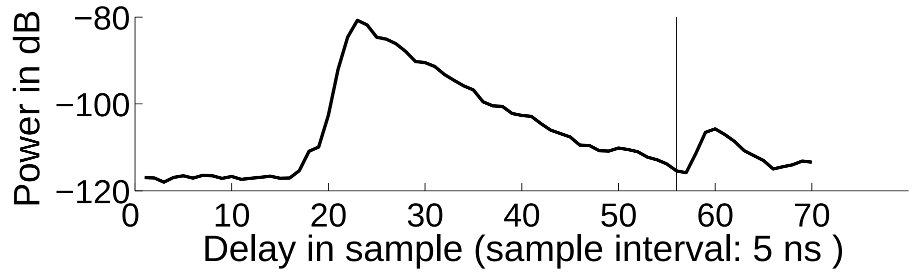

- Bartlett spectrum w.r.t. azimuth and elevation of departure at delay 280 ns:

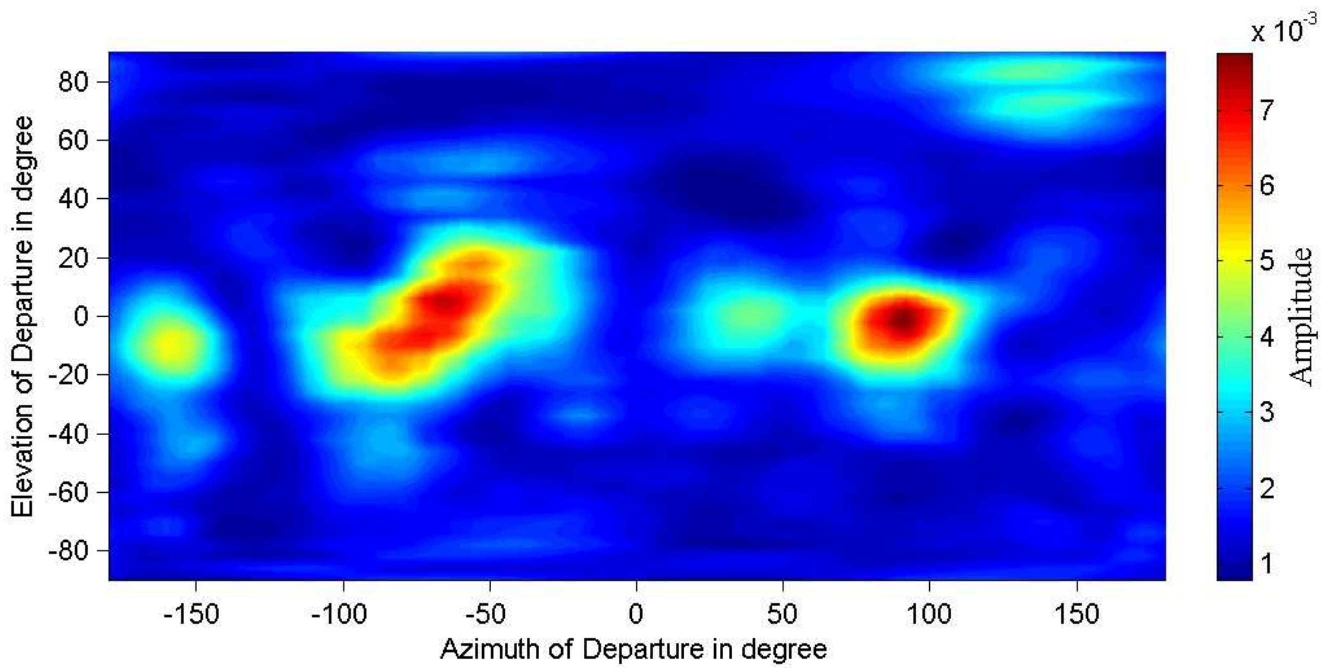

An experimental example: direction and delay dispersion of an indoor propagation channel

- Average delay power spectrum

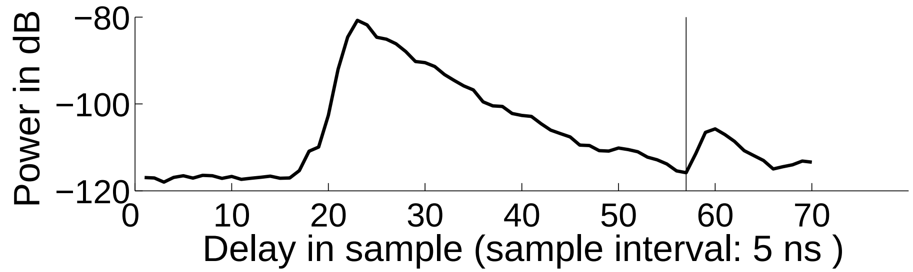

- Bartlett spectrum w.r.t. azimuth and elevation of departure at delay 285 ns:

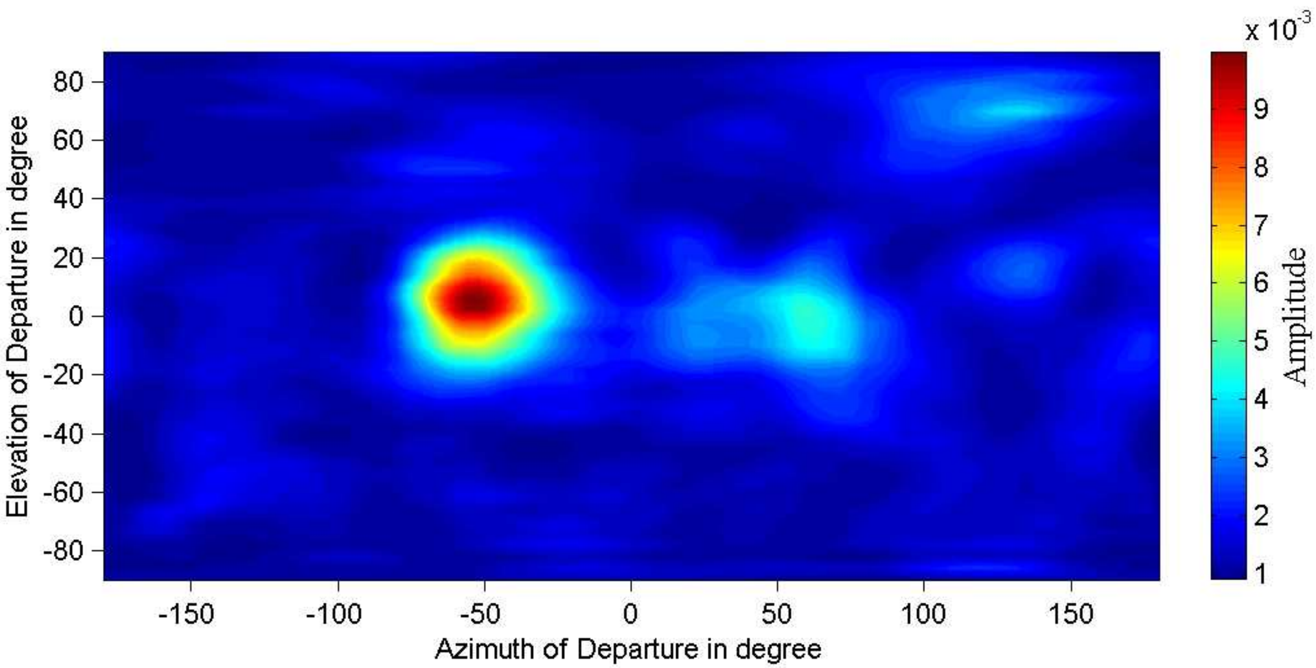

Signal Model

Received signal vector:

$$\boldsymbol{Y}(t) = \sum_{\ell=1}^{L} \boldsymbol{s}(t; \boldsymbol{\theta}_\ell) + \sqrt{\frac{N_0}{2}} \boldsymbol{W}(t),$$

where

- $\boldsymbol{Y}(t) \in \mathbb{C}^{M_2}$: output of the Rx array.
- $\boldsymbol{W}(t) \in \mathbb{C}^{M_2}$: circularly symmetric spatially and temporally white Gaussian noise with spectral height N_0.
- $\boldsymbol{s}(t; \boldsymbol{\theta}_\ell) \in \mathbb{C}^{M_2}$: signal contributed by the ℓth path at the output of the Rx array.

Signal Model

The signal contribution of individual specular path:

$$\begin{aligned}\boldsymbol{s}(t;\boldsymbol{\theta}_\ell) \doteq& [s_1(t;\boldsymbol{\theta}_\ell),\ldots,s_{M_2}(t;\boldsymbol{\theta}_\ell)]^{\mathrm{T}}\\ =& \exp\{j2\pi\nu_\ell t\}\boldsymbol{C}_2(\boldsymbol{\Omega}_{2,\ell})\boldsymbol{A}_\ell\boldsymbol{C}_1(\boldsymbol{\Omega}_{1,\ell})^T\boldsymbol{u}(t-\tau_\ell).\end{aligned}$$

with

- $\boldsymbol{\theta}_\ell \doteq [\boldsymbol{\Omega}_{1,\ell},\boldsymbol{\Omega}_{2,\ell},\tau_\ell,\nu_\ell,\boldsymbol{A}_\ell]$: parameter vector of the ℓth path;
- $\boldsymbol{C}_k(\boldsymbol{\Omega})\doteq[\boldsymbol{c}_{k,1}(\boldsymbol{\Omega}),\boldsymbol{c}_{k,2}(\boldsymbol{\Omega})] \in \mathbb{C}^{M_k\times 2},\ k{=}1,2$: response of Array k in direction $\boldsymbol{\Omega}$;
- $\boldsymbol{A}_\ell \doteq \begin{bmatrix}\alpha_{\ell,1,1} & \alpha_{\ell,1,2}\\ \alpha_{\ell,2,1} & \alpha_{\ell,2,2}\end{bmatrix} \in \mathbb{C}^{2\times 2}$: polarization matrix ;
- $\boldsymbol{u}(t) \doteq [u_1(t),\ldots,u_{M_1}(t)]^{\mathrm{T}} \in \mathbb{C}^{M_1}$: input signal vector.

Signal Model

Definition of a direction:

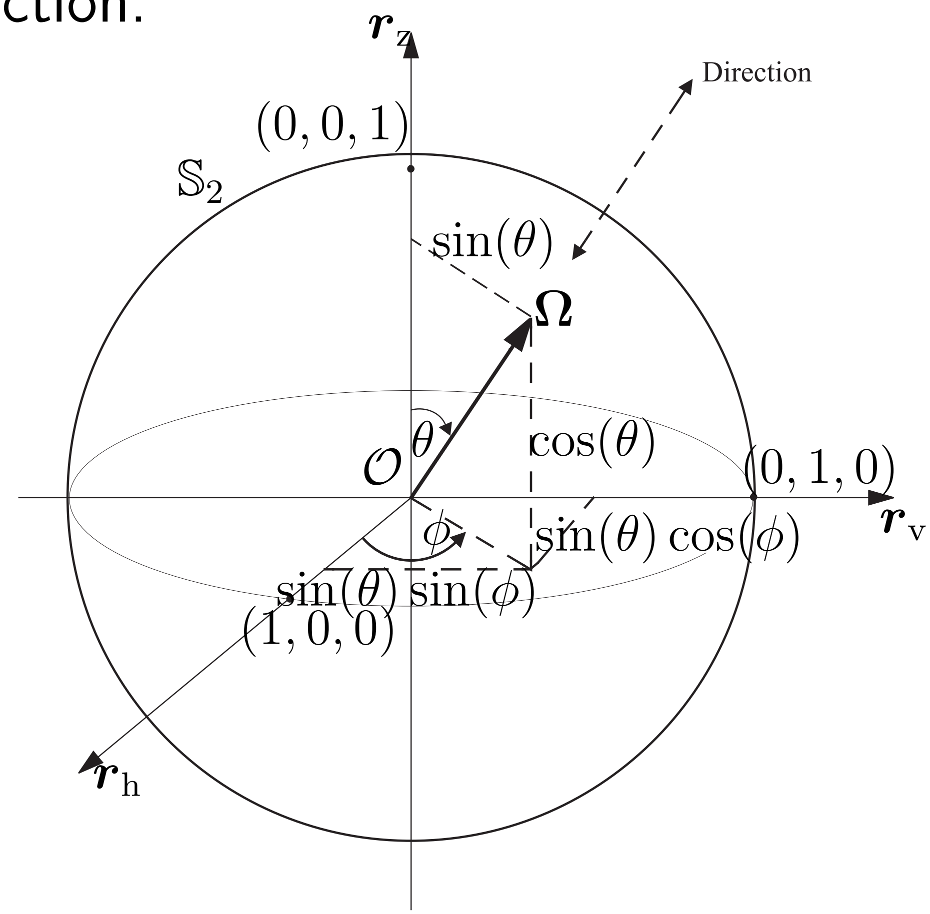

$$\boldsymbol{\Omega} = \boldsymbol{e}(\phi,\theta) \doteq [\cos(\phi)\sin(\theta), \sin(\phi)\sin(\theta), \cos(\theta)]^\mathrm{T} \in \mathbb{S}_2$$

The SAGE Algorithm

- Parameter vector:

$$\boldsymbol{\theta} \doteq [\boldsymbol{\theta}_1, ..., \boldsymbol{\theta}_L].$$

- Incomplete data: $\boldsymbol{Y}(t)$
- Hidden data: $\boldsymbol{x}_\ell(t)$

$$\boldsymbol{x}_\ell(t) \doteq \boldsymbol{s}(t; \boldsymbol{\theta}_\ell) + \sqrt{\frac{N_0}{2}} \boldsymbol{W}(t), \quad \ell = 1, \dots, L$$

(not the only choice)

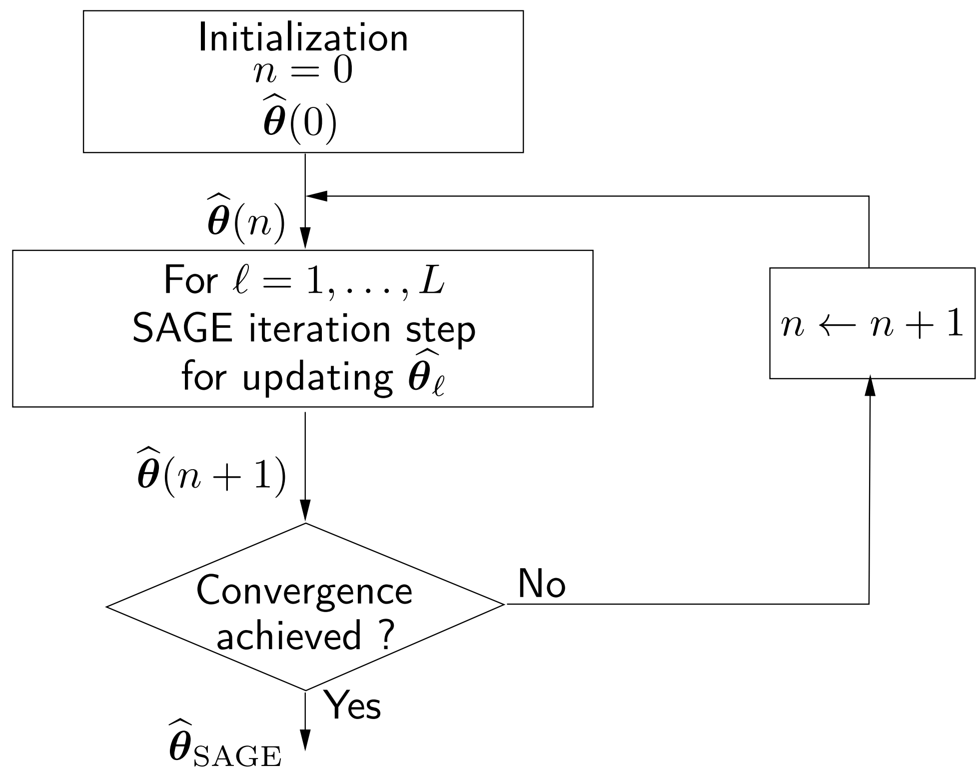

The SAGE Algorithm

- Expectation (E-) step:

$$\begin{aligned}\hat{\boldsymbol{x}}_\ell(t) &= \mathrm{E}[\boldsymbol{x}_\ell(t)|\boldsymbol{y}(t),\hat{\boldsymbol{\theta}}(n)] \\ &= \boldsymbol{y}(t) - \sum_{\ell'=1,\ell'\neq\ell}^{L} \boldsymbol{s}(t;\hat{\boldsymbol{\theta}}_{\ell'}(n))\end{aligned}$$

where $\hat{\boldsymbol{\theta}}(n)$ is the current estimate of $\boldsymbol{\theta}$.

The SAGE Algorithm

- Objective function maximized in the M-step:

$$z(\bar{\boldsymbol{\theta}}_\ell; x_\ell) \doteq \boldsymbol{f}(\bar{\boldsymbol{\theta}}_\ell)^{\mathrm{H}} \boldsymbol{D}(\boldsymbol{\Omega}_{2,\ell}, \boldsymbol{\Omega}_{1,\ell})^{-1} \boldsymbol{f}(\bar{\boldsymbol{\theta}}_\ell)$$

where

- $\bar{\boldsymbol{\theta}}_\ell \doteq [\boldsymbol{\Omega}_{1,\ell}, \boldsymbol{\Omega}_{2,\ell}, \tau_\ell, \nu_\ell]$;
- $\boldsymbol{D}(\boldsymbol{\Omega}_{2,\ell}, \boldsymbol{\Omega}_{1,\ell}) \doteq \left[\boldsymbol{C}_2(\boldsymbol{\Omega}_{2,\ell})^{\mathrm{H}}\ \boldsymbol{C}_2(\boldsymbol{\Omega}_{2,\ell})\right] \otimes \left[\boldsymbol{C}_1(\boldsymbol{\Omega}_{1,\ell})^{\mathrm{H}}\ \boldsymbol{C}_1(\boldsymbol{\Omega}_{1,\ell})\right]$;

The SAGE Algorithm

- Objective function maximized in the M-step:

$$z(\bar{\boldsymbol{\theta}}_\ell; x_\ell) \doteq \boldsymbol{f}(\bar{\boldsymbol{\theta}}_\ell)^{\mathrm{H}} \boldsymbol{D}(\boldsymbol{\Omega}_{2,\ell}, \boldsymbol{\Omega}_{1,\ell})^{-1} \boldsymbol{f}(\bar{\boldsymbol{\theta}}_\ell)$$

where

- $\boldsymbol{f}(\bar{\boldsymbol{\theta}}_\ell) \doteq \begin{bmatrix} \boldsymbol{c}_{2,1}^{\mathrm{H}}(\boldsymbol{\Omega}_{2,\ell}) \boldsymbol{X}_\ell(\tau_\ell, \nu_\ell) \boldsymbol{c}_{1,1}(\boldsymbol{\Omega}_{1,\ell})^* \\ \boldsymbol{c}_{2,1}^{\mathrm{H}}(\boldsymbol{\Omega}_{2,\ell}) \boldsymbol{X}_\ell(\tau_\ell, \nu_\ell) \boldsymbol{c}_{1,2}(\boldsymbol{\Omega}_{1,\ell})^* \\ \boldsymbol{c}_{2,2}^{\mathrm{H}}(\boldsymbol{\Omega}_{2,\ell}) \boldsymbol{X}_\ell(\tau_\ell, \nu_\ell) \boldsymbol{c}_{1,1}(\boldsymbol{\Omega}_{1,\ell})^* \\ \boldsymbol{c}_{2,2}^{\mathrm{H}}(\boldsymbol{\Omega}_{2,\ell}) \boldsymbol{X}_\ell(\tau_\ell, \nu_\ell) \boldsymbol{c}_{1,2}(\boldsymbol{\Omega}_{1,\ell})^* \end{bmatrix}.$
- $\boldsymbol{X}_\ell(\tau_\ell, \nu_\ell)$ is a $M_2 \times M_1$ dim. matrix with entries

$$X_{\ell,m_2,m_1}(\tau_\ell, \nu_\ell) = \sum_{i=1}^{I} \exp(-j2\pi\nu_\ell t_{i,m_2,m_1})$$

$$\cdot \int_0^{T_{\mathrm{sc}}} u^*(t-\tau_\ell) x_\ell(t + t_{i,m_2,m_1}) \mathrm{d}t,$$

The SAGE Algorithm

- Conditions for $\boldsymbol{D}(\boldsymbol{\Omega}_2, \boldsymbol{\Omega}_1)$ to be non-singular:

$$\det\big(\boldsymbol{D}(\boldsymbol{\Omega}_2, \boldsymbol{\Omega}_1)\big) \neq 0,$$

which holds, if and only if,

$$\boldsymbol{c}_{k,1}(\boldsymbol{\Omega}_k) \neq \gamma_k \cdot \boldsymbol{c}_{k,2}(\boldsymbol{\Omega}_k)$$

for some complex number $\gamma_k, k = 1, 2$.

  - A necessary and sufficient condition for $\boldsymbol{D}(\boldsymbol{\Omega}_2, \boldsymbol{\Omega}_1)$ to be always invertible is that the vectors $\boldsymbol{c}_{k,1}(\boldsymbol{\Omega}_k)$ and $\boldsymbol{c}_{k,2}(\boldsymbol{\Omega}_k), k = 1, 2$ are linearly independent for any $\boldsymbol{\Omega}_2$ and $\boldsymbol{\Omega}_1$.
  - When $\boldsymbol{D}(\boldsymbol{\Omega}_2, \boldsymbol{\Omega}_1)$ is non-invertible, the four coefficients in the polarization matrix $\boldsymbol{A}_\ell$ cannot be estimated separately.

The SAGE Algorithm

- Maximization (M-) step:

$$\begin{aligned}
\hat{\tau}_\ell'' &= \arg\max_{\tau_\ell} z(\hat{\phi}_{1,\ell}', \hat{\theta}_{1,\ell}', \hat{\phi}_{2,\ell}', \hat{\theta}_{2,\ell}', \tau_\ell, \hat{\nu}_\ell'; \hat{x}_\ell) \\
\hat{\nu}_\ell'' &= \arg\max_{\nu_\ell} z(\hat{\phi}_{1,\ell}', \hat{\theta}_{1,\ell}', \hat{\phi}_{2,\ell}', \hat{\theta}_{2,\ell}', \hat{\tau}_\ell'', \nu_\ell; \hat{x}_\ell) \\
\hat{\theta}_{2,\ell}'' &= \arg\max_{\theta_{2,\ell}} z(\hat{\phi}_{1,\ell}', \hat{\theta}_{1,\ell}', \hat{\phi}_{2,\ell}', \theta_{2,\ell}, \hat{\tau}_\ell'', \hat{\nu}_\ell''; \hat{x}_\ell) \\
\hat{\phi}_{2,\ell}'' &= \arg\max_{\phi_{2,\ell}} z(\hat{\phi}_{1,\ell}', \hat{\theta}_{1,\ell}', \phi_{2,\ell}, \hat{\theta}_{2,\ell}'', \hat{\tau}_\ell'', \hat{\nu}_\ell''; \hat{x}_\ell) \\
\hat{\theta}_{1,\ell}'' &= \arg\max_{\theta_{1,\ell}} z(\hat{\phi}_{1,\ell}', \theta_{1,\ell}, \hat{\phi}_{2,\ell}'', \hat{\theta}_{2,\ell}'', \hat{\tau}_\ell'', \hat{\nu}_\ell''; \hat{x}_\ell) \\
\hat{\phi}_{1,\ell}'' &= \arg\max_{\phi_{1,\ell}} z(\phi_{1,\ell}, \hat{\theta}_{1,\ell}'', \hat{\phi}_{2,\ell}'', \hat{\theta}_{2,\ell}'', \hat{\tau}_\ell'', \hat{\nu}_\ell''; \hat{x}_\ell). \\
\boldsymbol{\alpha}_\ell'' &= (IPT_{\mathrm{sc}})^{-1} \boldsymbol{D}(\boldsymbol{\Omega}_{2,\ell}'', \boldsymbol{\Omega}_{1,\ell}'')^{-1} \boldsymbol{f}(\bar{\boldsymbol{\theta}}_\ell'')
\end{aligned}$$

$$\boldsymbol{\alpha}_\ell \doteq \mathrm{vec}(\boldsymbol{A}_\ell)$$

Initialization

- Successive Interference Cancellation:

$$y^{(\ell)}(t) = y(t) - \sum_{\ell'=1}^{\ell-1} s(t; \hat{\boldsymbol{\theta}}_{\ell'}(0))$$

- Non-Coherent Maximum Likelihood (NC-ML) estimator for initializing $\hat{\tau}_\ell$, $\hat{\nu}_\ell$, and $\hat{\boldsymbol{\Omega}}_{2,\ell}$.

- Coherent Maximum Likelihood (C-ML) estimator for initializing $\hat{\boldsymbol{\Omega}}_{1,\ell}$ and $\hat{\boldsymbol{\alpha}}_\ell$.

Initialization

- NC-ML estimate of delay τ_ℓ

$$\hat{\tau}_\ell(0) = \arg\max_{\tau_\ell}\left\{\sum_{i=1}^{I}\sum_{m_2=1}^{M_2}\sum_{m_1=1}^{M_1}\left|\int_0^{T_{\mathrm{sc}}} y^{(\ell)}(t+t_{i,m_2,m_1})u^*(t-\tau_\ell)\mathrm{d}t\right|^2\right\}.$$

- NC-ML estimate of Doppler frequency ν_ℓ:

$$\hat{\nu}_\ell(0) = \arg\max_{\nu_\ell}\left\{\sum_{m_2=1}^{M_2}\sum_{m_1=1}^{M_1}\left|\sum_{i=1}^{I}\exp(-j2\pi\nu_\ell t_{i,m_2,m_1})\right.\right.$$

$$\left.\left.\cdot\int_0^{T_{\mathrm{sc}}} y^{(\ell)}(t+t_{i,m_2,m_1})u^*\big(t-\hat{\tau}_\ell(0)\big)\mathrm{d}t\right|^2\right\}.$$

Initialization

- NC-ML estimate of direction of arrival $\mathbf{\Omega}_{2,\ell}$:

$$\hat{\mathbf{\Omega}}_{2,\ell}(0) = \arg\max_{\mathbf{\Omega}_{2,\ell}} \Bigg\{ \sum_{m_1=1}^{M_1} \Bigg[\left| \tilde{\boldsymbol{c}}_{2,1}^{\mathrm{H}}(\mathbf{\Omega}_{2,\ell}) \boldsymbol{y}_{m_1}^{(\ell)} \right|^2 + \left| \tilde{\boldsymbol{c}}_{2,2}^{\mathrm{H}}(\mathbf{\Omega}_{2,\ell}) \boldsymbol{y}_{m_1}^{(\ell)} \right|^2$$
$$-2\mathcal{R}\{ \boldsymbol{y}_{m_1}^{(\ell)H} \tilde{\boldsymbol{c}}_{2,2}(\mathbf{\Omega}_{2,\ell} \tilde{\boldsymbol{c}}_{2,1}^{\mathrm{H}}(\mathbf{\Omega}_{2,\ell}) \boldsymbol{y}_{m_1}^{(\ell)H} \tilde{\boldsymbol{c}}_{2,2}^{\mathrm{H}}(\mathbf{\Omega}_{2,\ell}) \tilde{\boldsymbol{c}}_{2,1}(\mathbf{\Omega}_{2,\ell}) \} \Bigg] \Bigg\}.$$

- C-ML Estimate of direction of departure $\mathbf{\Omega}_{1,\ell}$:

$$\hat{\mathbf{\Omega}}_{1,\ell}(0) = \arg\max_{\mathbf{\Omega}_{1,\ell}} \left\{ z\left(\hat{\mathbf{\Omega}}_{2,\ell}(0), \mathbf{\Omega}_{1,\ell}, \hat{\tau}_\ell(0), \hat{\nu}_\ell(0); \hat{y}_\ell \right) \right\}$$

- C-ML Estimate of the complex polarization vector $\boldsymbol{\alpha}_\ell$

$$\hat{\boldsymbol{\alpha}}_\ell(0) = (IPT_{\mathrm{sc}})^{-1} \boldsymbol{D}\left(\hat{\mathbf{\Omega}}_{2,\ell}(0), \hat{\mathbf{\Omega}}_{1,\ell}(0) \right)^{-1} \boldsymbol{f}\left(\hat{\bar{\boldsymbol{\theta}}}_\ell(0) \right)$$

Experimental Investigations

Characteristics of the measurement setup:

- MIMO channel sounder: Propsound
- Tx Array: 3x8 omni-directional dual-polarized array (M_1=54),
- Rx Array: 4x4 planar dual-polarized array (M_2=32),
- 2.45 GHz Carrier frequency and 100 MHz bandwidth

Tx

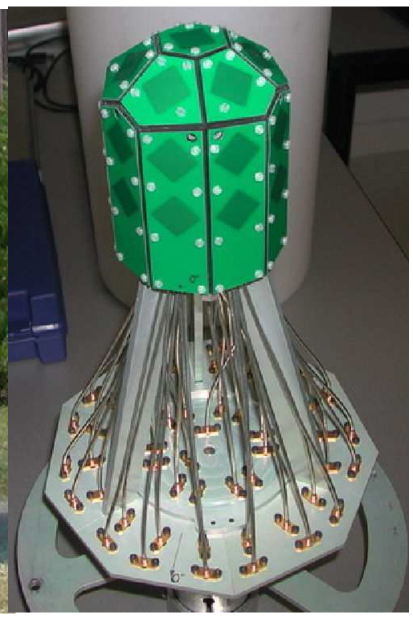

Tx Array

Rx

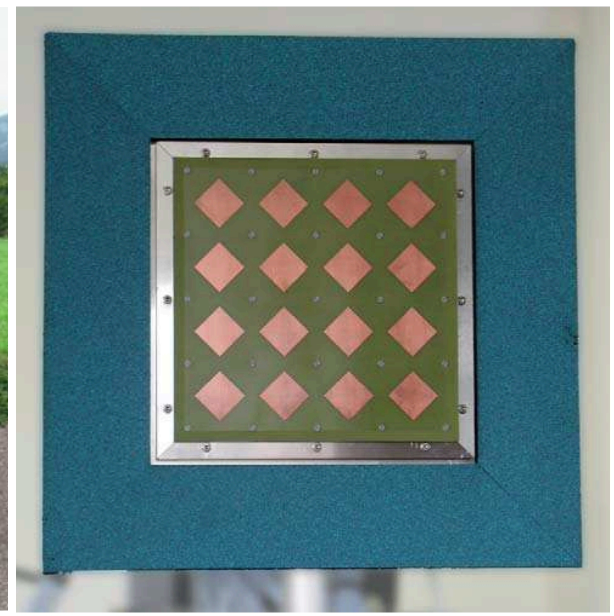

Rx Array

Experimental Investigations

Investigated propagation environment:

Surrounding of the Rx

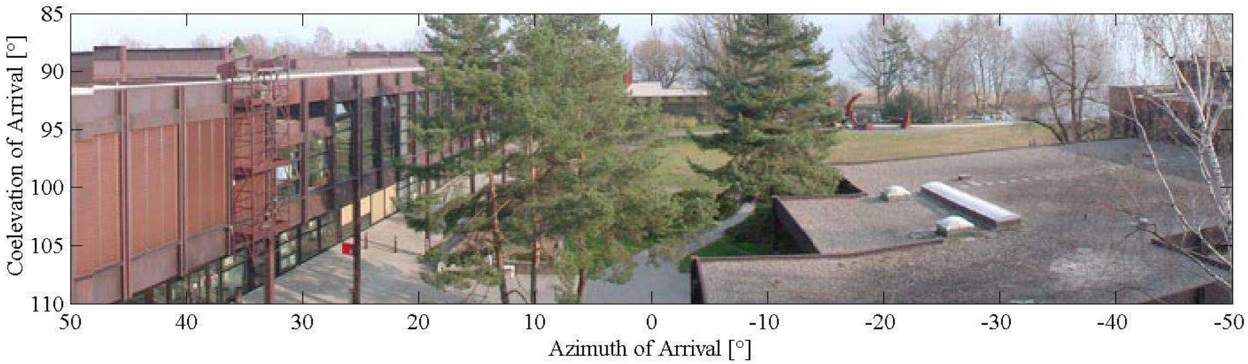

Surrounding of the Tx

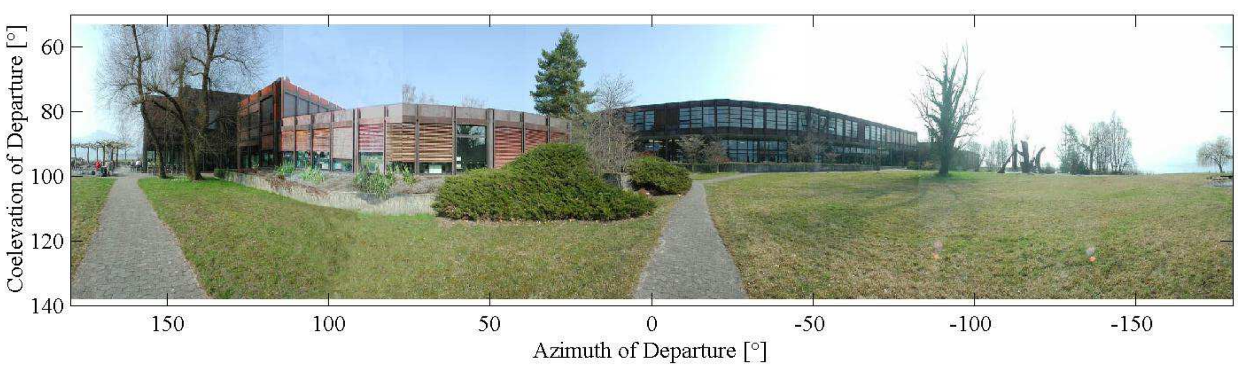

Map of the environment

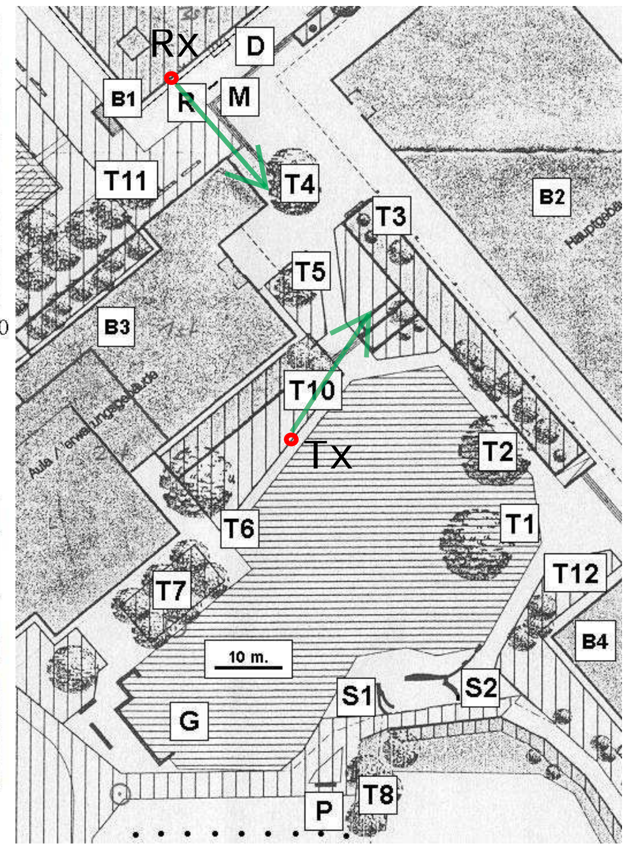

Experimental Investigations (NLOS)

Estimated Directions of Arrival (DoAs)

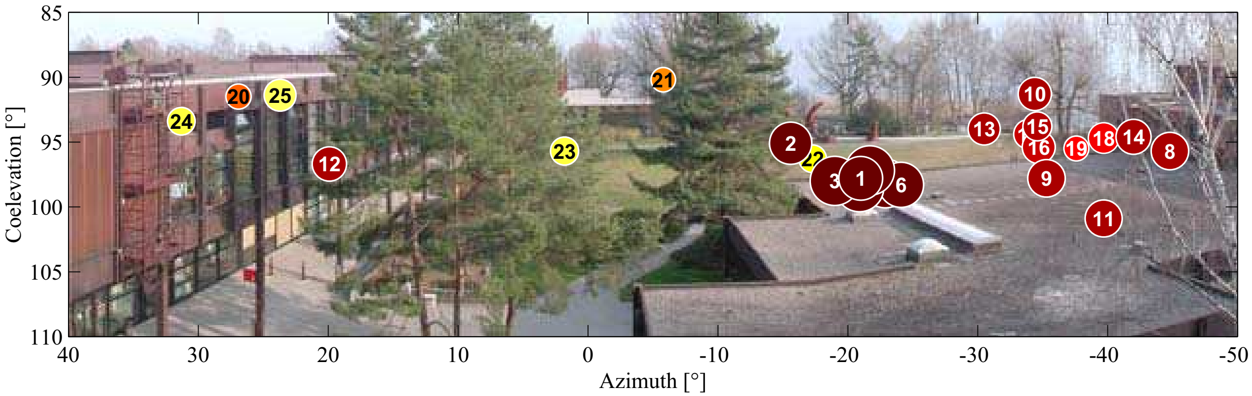

Estimated Directions of Departure (DoDs)

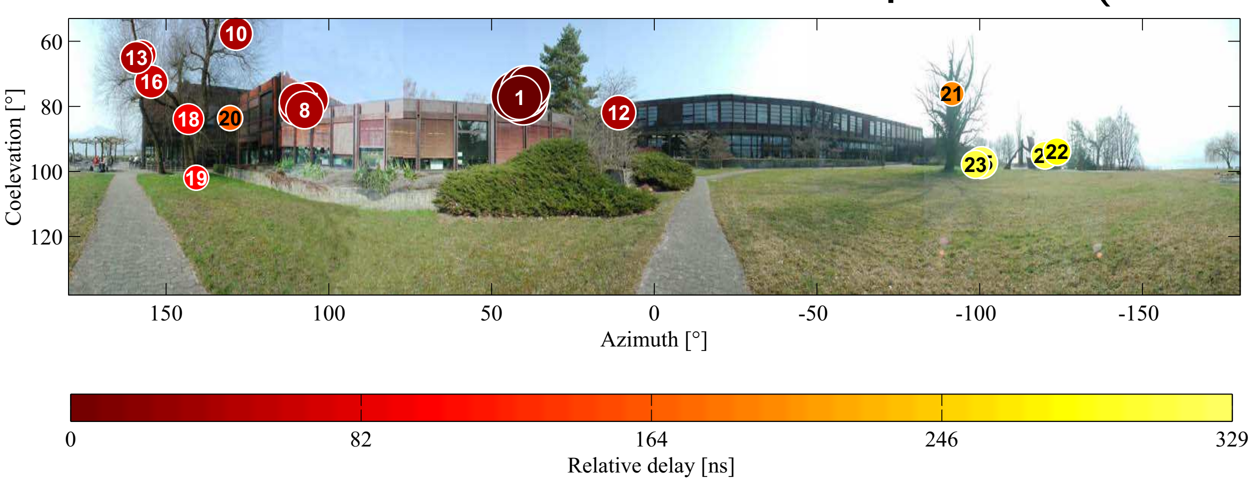

Reconstructed Paths

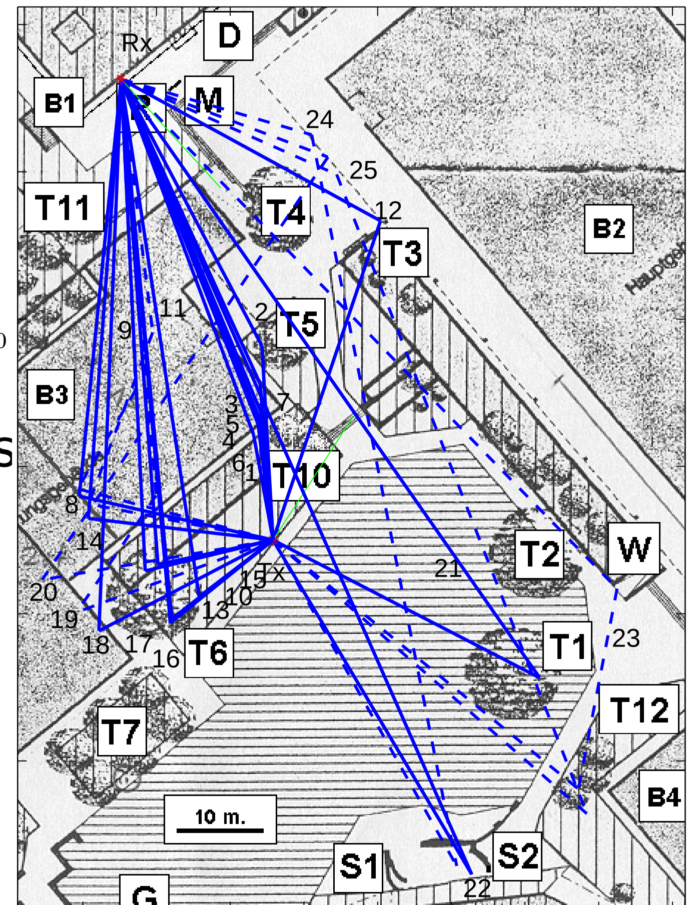

Experimental Investigations (NLOS)

Estimated Directions of Arrival (DoAs)

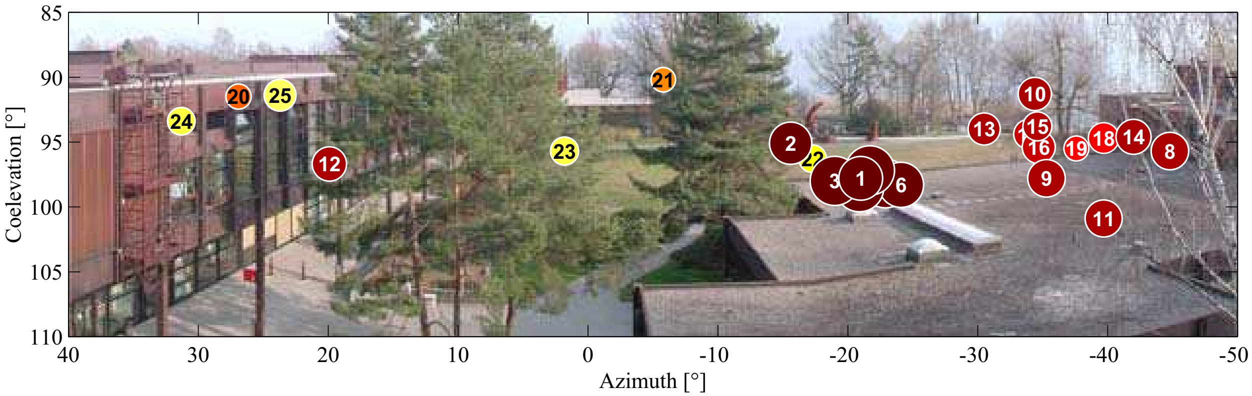

Reconstructed Path 21

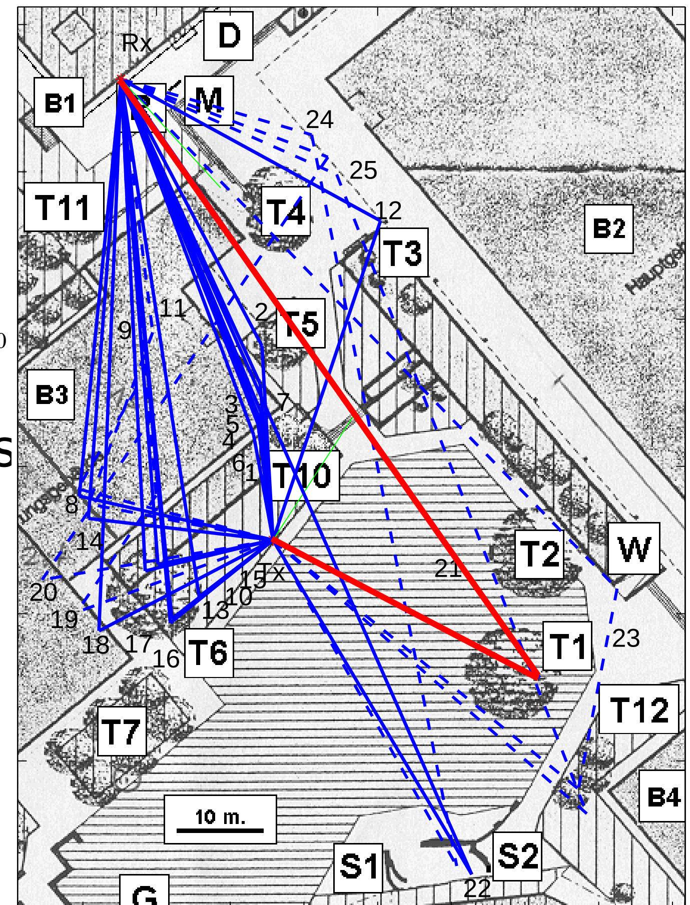

Estimated Directions of Departure (DoDs)

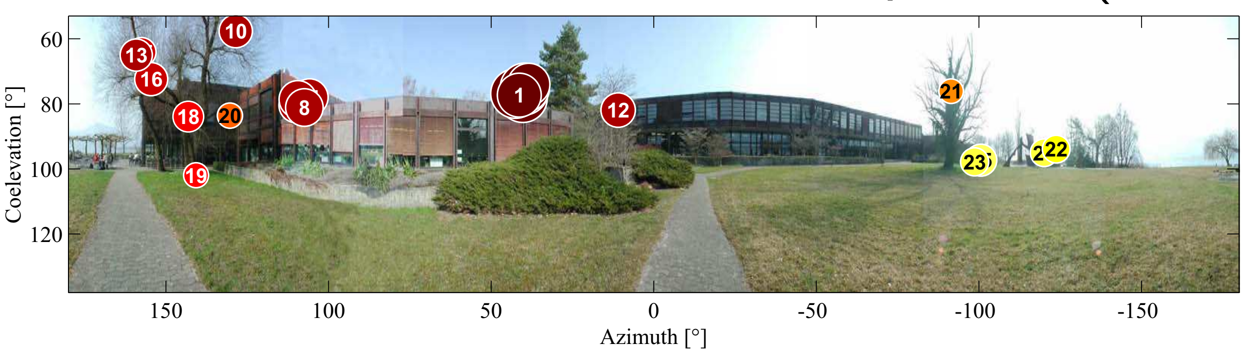

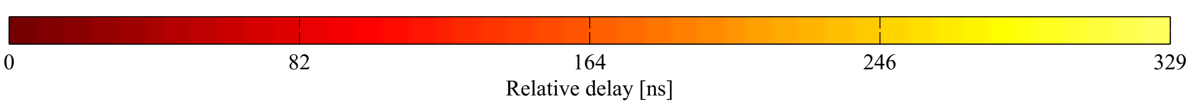

Experimental Investigations (NLOS)

Estimated Directions of Arrival (DoAs)

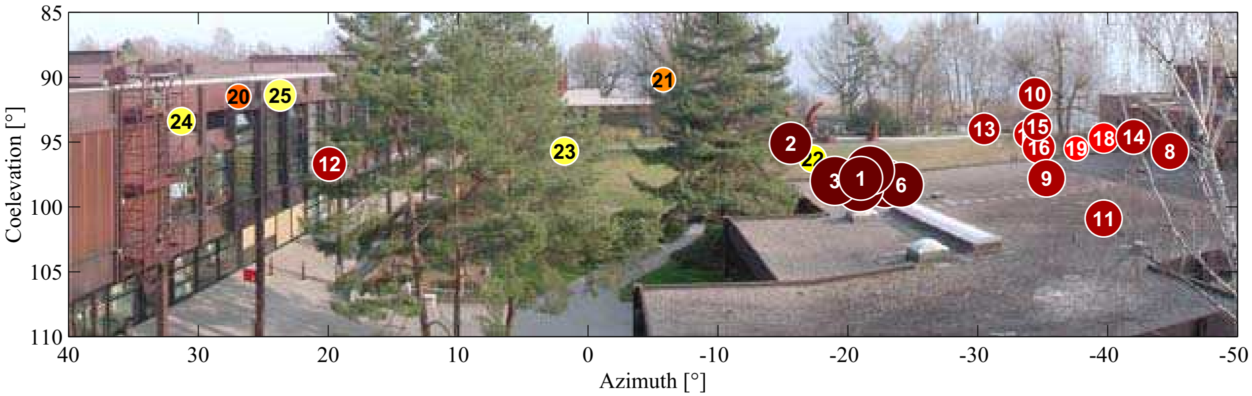

Estimated Directions of Departure (DoDs

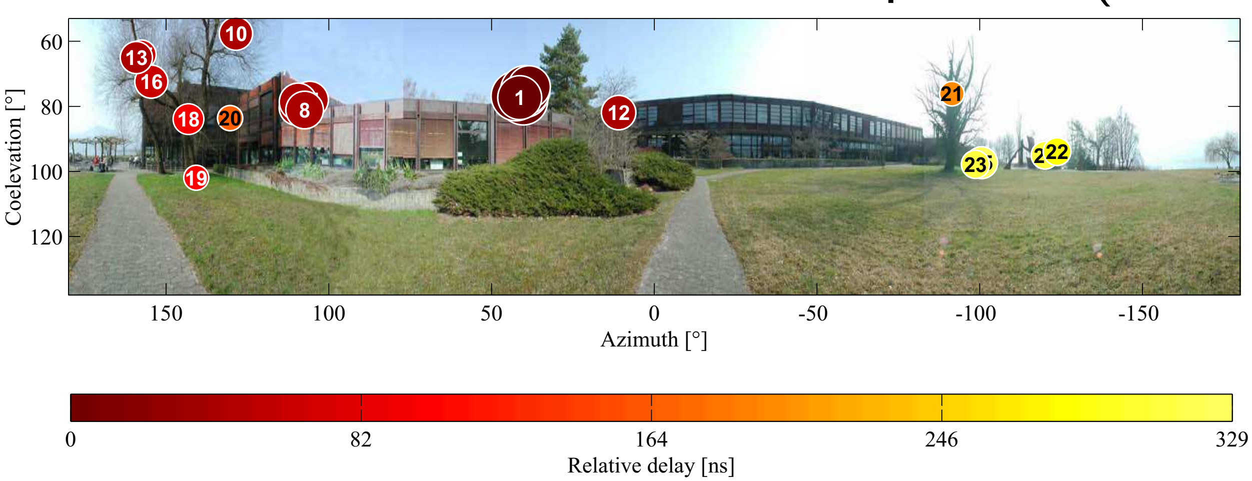

Reconstructed Path 24

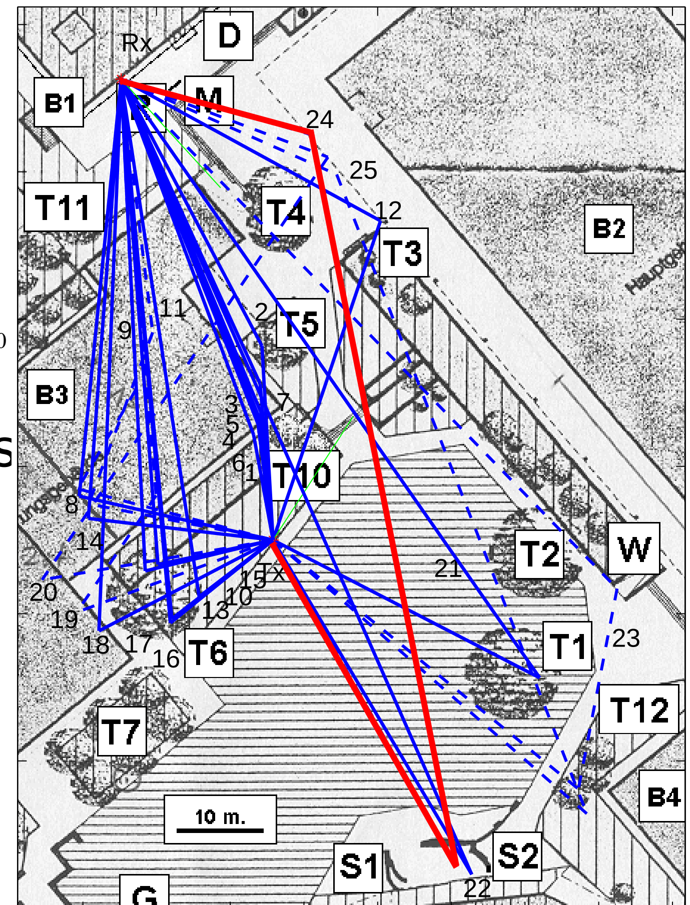

Experimental Investigations (NLOS)

Estimated polarization:

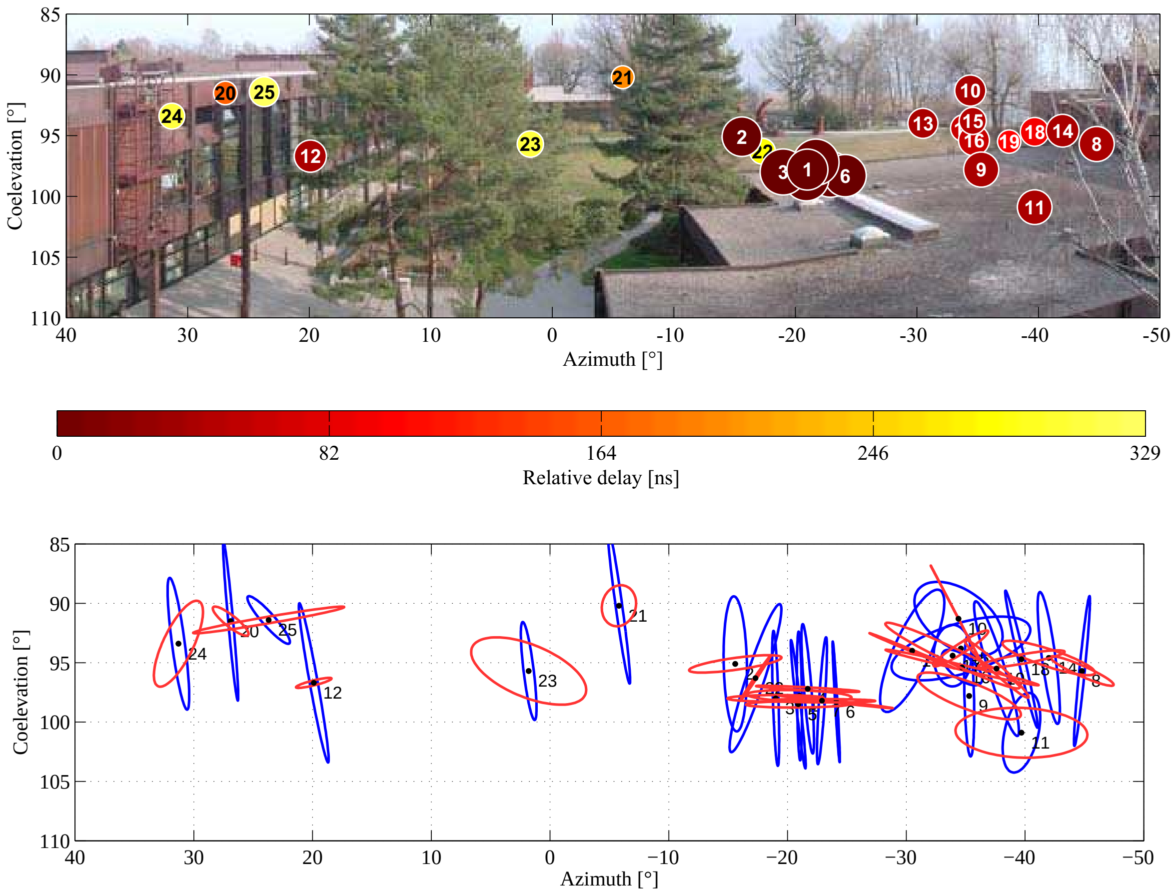

- Blue ellipses : polarization ellipses calculated using $\begin{bmatrix}\hat{a}_{d,1,1} & \hat{a}_{d,2,1}\end{bmatrix}^{\mathrm{T}}$,
- Red ellipses : polarization ellipses calculated using $\begin{bmatrix}\hat{a}_{d,1,2} & \hat{a}_{d,2,2}\end{bmatrix}^{\mathrm{T}}$.

Experimental investigations (NLOS)

Scatter plot of the estimated cross-polarization discrimination (XPD) of the individual paths:

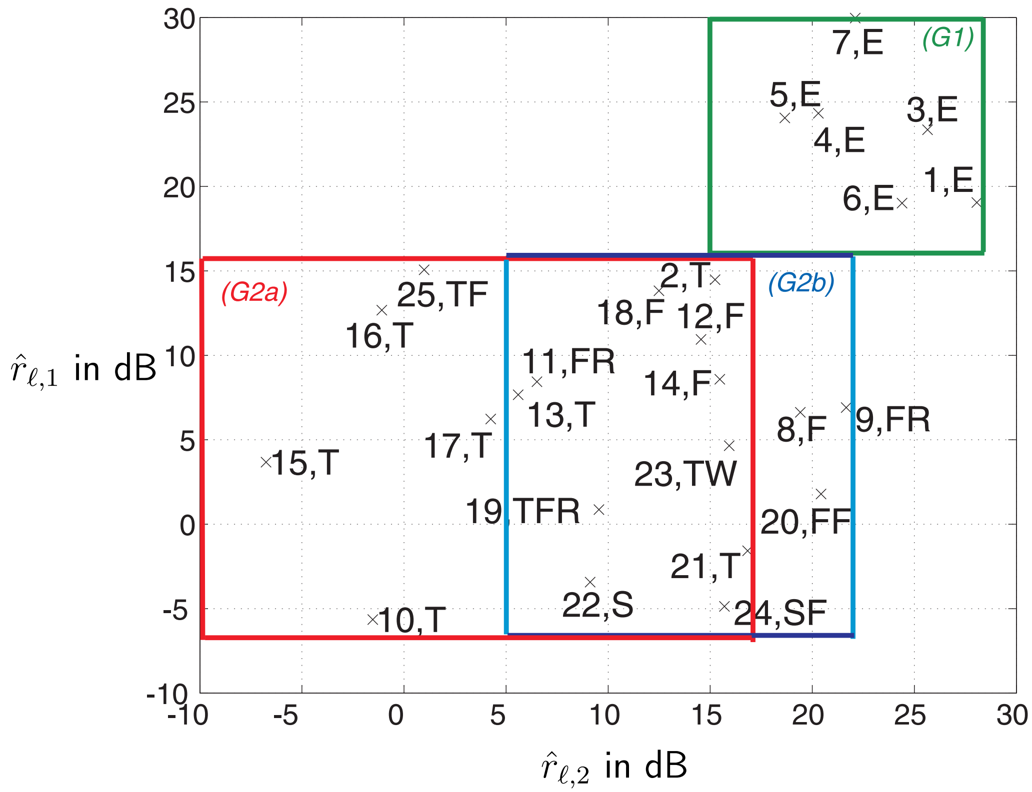

- $\hat{r}_{\ell,1} = \left|\hat{\alpha}_{\ell,1,1}/\hat{\alpha}_{\ell,2,1}\right|^2$ and $\hat{r}_{\ell,2} = \left|\hat{\alpha}_{\ell,2,2}/\hat{\alpha}_{\ell,1,2}\right|^2$
- The symbols denote the types of scatterers identified along the paths: facade (F), roof (R), edge (E) of buildings as well as tree (T), sculpture (S), and wall (W).

Experimental investigations (NLOS)

XPDs versus the interaction type:

Group	Interaction type/scatterers along the propagation path	XPDs in dB	
		$\hat{r}_{\ell,1}$	$\hat{r}_{\ell,2}$
1	Diffraction around the roof edge of B3	$[15, 28]$	$[16, 30]$
2a	Reflection/scattering by at least one tree	$[-10, 17]$	$[-6, 16]$
2b	Reflection/scattering only by man-made structures	$[5, 22]$	$[-6, 16]$

Experimental investigations (LOS)

Directions of incidence (top) and directions of departure (bottom):

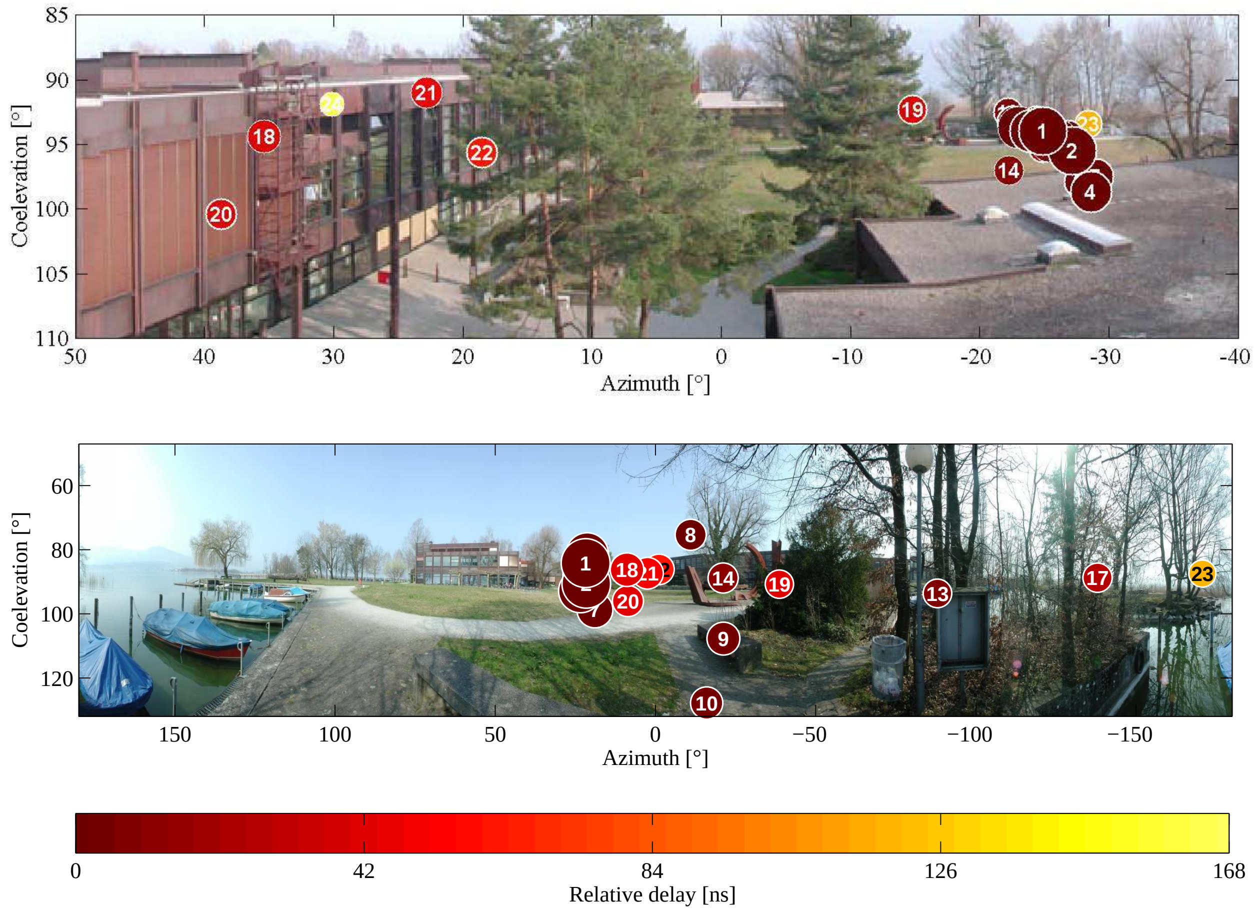

Experimental investigations (LOS)

Estimated polarization:

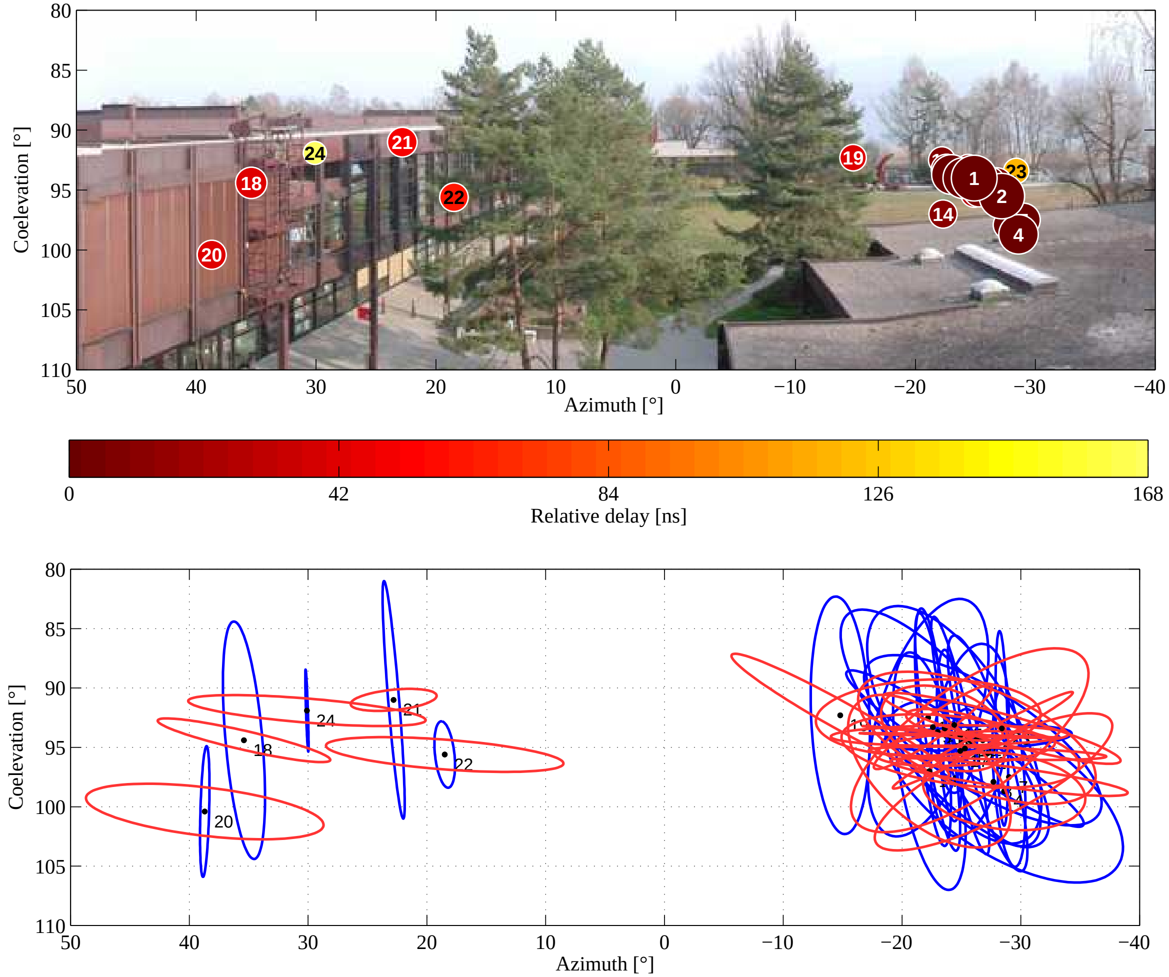

Experimental investigations (LOS)

Reconstructed one-bounce (left) and two-bounce (right) propagation paths:

Experimental investigations (LOS)

Scatter plot of the estimated cross-polarization discrimination (XPD) of the individual paths:

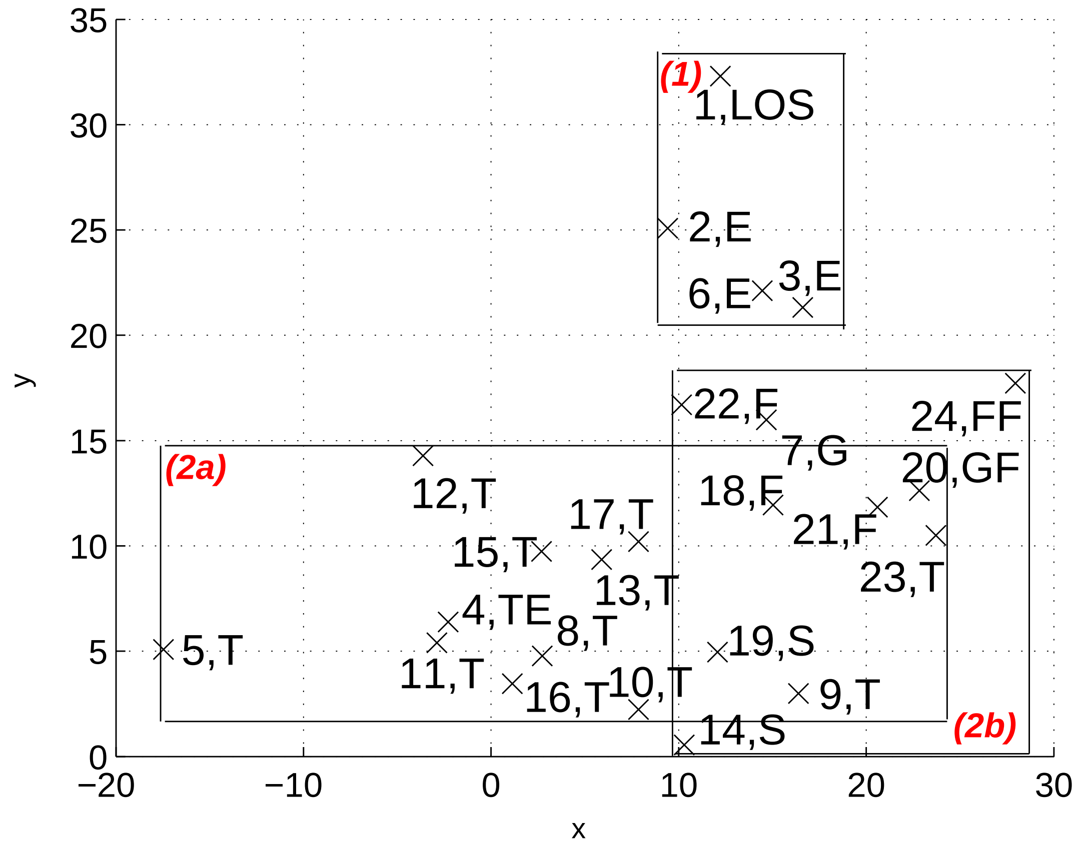

The symbols denote the types of scatterers identified along the paths: facade (F), roof (R), edge (E) of buildings as well as tree (T), sculpture (S), ground (G) and wall (W).

Experimental investigations (LOS)

XPDs versus the interaction type:

Group	Interaction type along the propagation path	XPDs in dB	
		$\hat{r}_{\ell,1}$	$\hat{r}_{\ell,2}$
1	LOS and diffraction by the roof edge of B3	$[9, 17]$	$[21, 33]$
2a	Reflection/scattering by at least one tree	$[-18, 24]$	$[2, 15]$
2b	Reflection/scattering only by man-made structures	$[10, 28]$	$[0, 17]$

Experimental investigations (LOS)

Scatter plot of the estimated singular values of the individual paths:

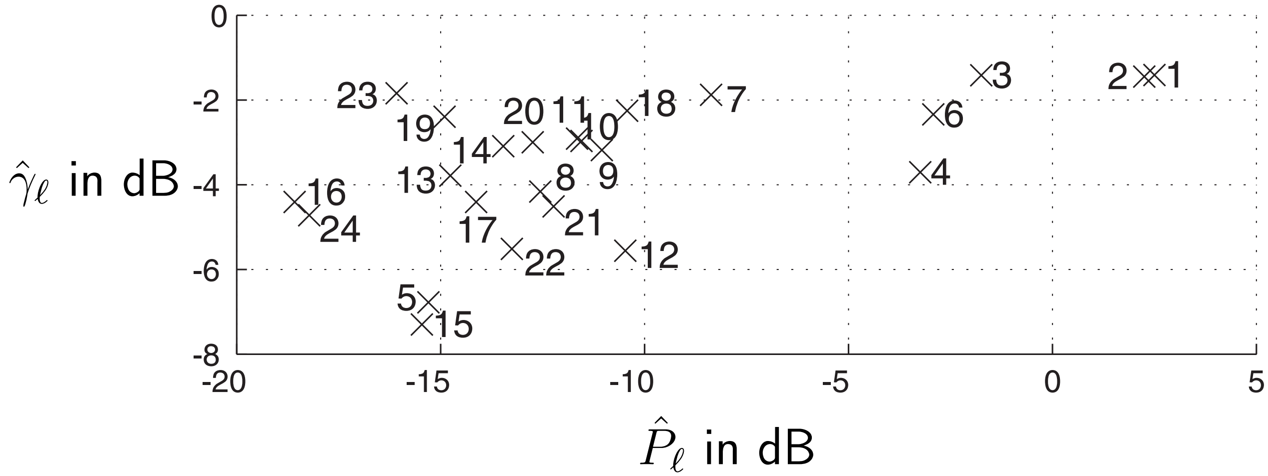

- $\hat{\gamma}_\ell = \hat{\varsigma}_{\ell,\min}/\hat{\varsigma}_{\ell,\max}$:
  - $\hat{\varsigma}_{\ell,\min}$: minimum of the estimated singular values of $\hat{\boldsymbol{A}}_\ell$
  - $\hat{\varsigma}_{\ell,\max}$: maximum of the estimated singular values of $\hat{\boldsymbol{A}}_\ell$
- $\hat{P}_\ell \doteq \hat{\varsigma}^2_{\ell,\min} + \hat{\varsigma}^2_{\ell,\max}$: the estimated total path gain

.

Conclusions

- A SAGE algorithm is derived for estimation of path parameters: directions of departure, directions of arrival, propagation delay, Doppler frequency, and polarization matrix.
- A detailed insight into the propagation mechanisms is obtained by exploring the polarization characteristics of individual propagation path:
  - Identify the type of scatterers and interactions;
  - Relate the polarization characteristics of the paths to the interaction types.
- This insight is of paramount importance
  - For the design of realistic stochastic models of the propagation channel for MIMO system applications;
  - To enhance the prediction accuracy of deterministic models for field prediction.